Thin-Walled Structures 186 (2023) 110717

Contents lists available at ScienceDirect

Thin-Walled Structures

journal homepage: www.elsevier.com/locate/tws

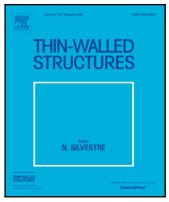

Full length article

Numerical investigation and design for the local buckling behaviour of high strength steel hexagonal hollow section stub columns under axial compression

Jun-zhi Liu [a,1], Han Fang [b,*], Jiachen Guo [c], Shuai Li [c], Tak-Ming Chan [c,d]

[a] School of National Safety and Emergency Management, Beijing Normal University, Zhuhai, China
[b] School of Civil Engineering, University of Leeds, Leeds, United Kingdom
[c] Department of Civil and Environmental Engineering, The Hong Kong Polytechnic University, Hong Kong, China
[d] Chinese National Engineering Research Centre for Steel Construction (Hong Kong Branch), The Hong Kong Polytechnic University, Hong Kong, China

ARTICLE INFO

Keywords:
High strength steel
Local buckling behaviour
Hexagonal hollow section stub columns
Numerical modelling
Design approaches

ABSTRACT

The local buckling behaviour of high strength steel (HSS) hexagonal hollow section (HexHS) stub columns encompassing three different fabrication routes under axial compression is numerically investigated in this study. Finite-element (FE) models were developed and validated against the experimental results. The validated FE models were subsequently employed to carry out parametric studies to expand structural performance data covering a wider range of geometries and cross-section slenderness as well as two different steel grades. The obtained results from FE models in line with the experimental data were used to evaluate the applicability of the existing design codes and the design approaches in literature to HSS HexHS under pure compression. The comparison indicates that the current slenderness yield limiting values in design codes cannot be simply extended to HSS HexHS stub columns. All the design codes exhibit a high degree of conservatism due to the lack of consideration for strain hardening whereas the Continuous Strength Method (CSM) was found to provide more accurate predictions than the Direct Strength Method (DSM). Modified design approaches are proposed to improve the accuracy of the strength predictions for HSS HexHS stub columns.

1. Introduction

Steel tubular sections are widely adopted in the construction industry for infrastructures such as buildings, bridges and offshore structures because of the aesthetic appearance and great local or torsional buckling resistance [1–3]. With the advancement of material technology, high strength steel materials are readily available in the market and produced through Thermal Mechanically Controlled Process (TMCP) and Quenched and Tempered (QT) methods to obtain good ductility and weldability [4–6]. The application of HSS in structural components leads to lighter structural members, reduced member sizes and lower costs for transportation and erection due to high strength-to-weight ratios of HSS. In addition, the environmental benefits of using HSS members in buildings have been demonstrated from the structural design practice for the multi-purpose Stadium Friends Arena in Stockholm, as shown in Fig. 1. The use of HSS members for this stadium led to the reduction of global warming potential of 17% compared with that based on the design using normal strength steel (NSS) [3] for the members.

In order to implement structural components made from HSS, numerous research investigations have been carried out to examine the structural performance of welded and cold-formed HSS tubular section members subjected to various loading conditions. Nevertheless, most of the previous research studies focus on members with conventional tubular cross-sections including rectangular-(RHS), square-(SHS), [7–20] circular-(CHS) [21–26], and elliptical hollow sections (EHS) [27–30]. In addition to these cross-sectional shapes, structural members of novel shapes with combined structural efficiency and architectural aesthetics are formed and investigated. Specifically, cold-formed steel oval hollow sections have been investigated and cold-formed semi-oval hollow sections have also been studied in [31–33]. In recent years, there have been growing interests into the applications of polygonal sections such as HSS hexagonal-(HexHS) [34,35], irregular hexagonal-(IHexHS) [36–38], octagonal- (OctHS) [39,40] and irregular octagonal hollow sections (IOctHS) [41]. The advantages of using HexHS/IHexHS and OctHS/IOctHS can be illustrated that the width of the flat portion is smaller than the counterparts of square and rectangular hollow sections (SHS/RHS) if they are delivered with similar perimeters, therefore

* Corresponding author.
E-mail address: h.fang1@leeds.ac.uk (H. Fang).
[1] Formerly, Department of Civil and Environmental Engineering, The Hong Kong Polytechnic University, Hong Kong, China.

https://doi.org/10.1016/j.tws.2023.110717
Received 14 January 2023; Received in revised form 12 March 2023; Accepted 16 March 2023
Available online xxxx

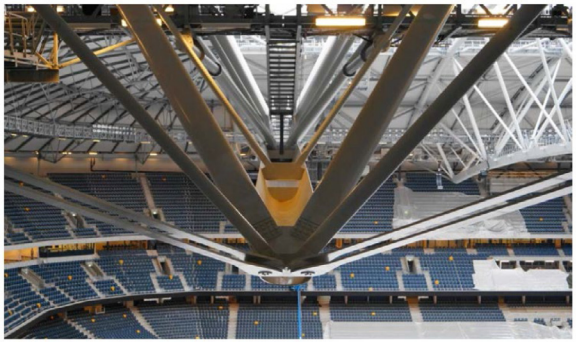

Fig. 1. Roof truss of multi-purpose stadium Friends Arena in Stockholm [3].

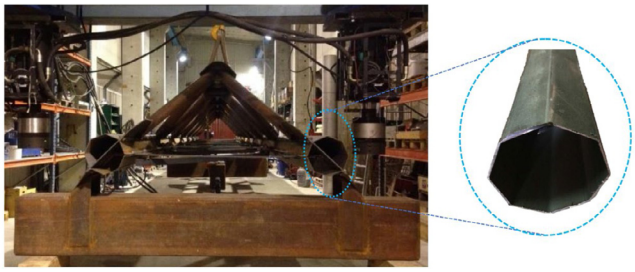

Fig. 2. Octagonal hollow sections adopted in a novel truss system [3].

exhibiting stronger local buckling resistance than that of SHS and RHS. In addition, the flat surfaces allow for easier connection by providing an operating platform for welding, as well as bolted connection with end plate or gusset plate. Moreover, the newly emerged structural systems, such as modular integrated construction (MIC) propose higher requirement on the versatility of the structural configurations and connection possibilities. For instance, a novel roof truss systems adopted polygonal sections of OctHS/IOctHS as compression chord members to facilitate structural efficiency, as shown in Fig. 2.

In addition to the structural applications of steel structures, HexHS have also been employed in high-rise buildings as exterior mega-columns by filling concrete into the tubes to provide multi-directional connection and resist the vertical heavy loads as composite structures [42]. Though prominent advantages of HexHS are recognised, limited studies have been performed for HSS HexHS, underlying the necessities to systematically explore the structural behaviour of HSS HexHS structures.

Conventional tubular profiles of SHS, RHS, and CHS are codified in current design codes including AISI/AISC 360-16 [43], AS 4100 [44] and EN 1993-1-1 [45]. The design specifications for HexHS can only be found in ASCE/SEI 48-11 [46] with cross-sectional resistance design equations provided without distinguishing fabrication routes. To allow for the design of HSS members, EN 1993-1-12 [47] specifies the applicable range of strength grade up to S700 with nominal yield strength of 700 MPa, and the American design code of AISI/AISC 360-16 [43] and AS 4100 [44] provide the design guidelines for steel with yield strength up to 690 MPa. However, it should be noted that these two design provisions cannot be directly applied to hollow sections because of the more stringent requirements stipulated in AISI/AISC 360-16 [43] and AS 4100 [44]. Specifically, hollow sections with nominal yield strengths of 485 MPa and 450 MPa are stipulated as the upper bound for hollow sections design in AISI/AISC 360-16 [43] and AS 4100 [44] respectively. Hence, the applicability and suitability of the existing design codes to the HexHS stub columns need to be assessed and evaluated.

To better understand the structural behaviour and develop a safe and economical design of HSS HexHS structures, numerical investigations of local buckling performance of HSS HexHS subjected to axial compression with three different fabrication routes are presented in this paper. The three fabrication routes comprise W-series, CF-1 series and CF-2 series, where W-series refer to the sections with six plates welded together and CF-1 series refer to the sections formed by welding two cold-formed sections with each half with two bent-corners. CF-2 series sections are those formed by welding two cold-formed part with each half featuring three bent-corners. The detailed fabrication information can be found in [34].

The numerical investigations presented in this paper are based upon the experimental study on 18 HSS Q690 HexHS stub columns carried out by the authors [35] with a large spectrum of cross-section dimensions (side width to thickness, (b/t) varying from 7.6 to 31.9. The finite element (FE) models were firstly developed and validated against the experimental test results. Based upon the validation of FE models, extensive parametric studies were carried out to cover a larger range of cross-section dimensions with different steel grades. The experimental and numerical results for HexHS under concentric compression were used to assess the suitability of the existing structural steel design codes of EN 1993-1-1 [45], EN, 1993-1-5 [48], EN 1993-1-12 [47], AISI/AISC 360-16 [43] and AS 4100 [44] as well as the advanced design approaches of Direct Strength Method (DSM), and Continuous Strength Method (CSM).

2. Numerical investigation

2.1. General

Numerical analysis was carried out using the commercially available finite element program package ABAQUS [49]. The modelling techniques for FE models of HSS HexHS with different fabrication routes were introduced. The experimental results from previous studies in [35] were used to confirm the validity of the developed FE models. The subsequent parametric studies were conducted based on the validated FE models.

2.2. Development of FE models

Detailed modelling techniques developed for HSS HexHS stub columns are presented in this section. The reduced integration four-noded doubly curved shell element S4R was employed to model the HSS HexHS stub columns, which has been successfully applied and used in FE modelling to predict the structural responses of various hollow sections structures with different cross-sectional shapes [41,50]. Mesh sensitivity studies were carried out to determine an appropriate element size and mesh density to provide accurate predictions while minimising computational cost. Hence, an average element size equal to one twentieth of the largest plate width ($b_s/20$) was adopted for the flat parts of the cross-sections whereas finer mesh with the element size of one thirtieth of the largest plate width ($b_s/30$) was employed to account for the curved geometries of the corner regions due to the cold-forming process. For the cross-sections with welding details, particular attention was paid to ensure that the geometries and properties of the butt welding (i.e., all corner regions of W-series cross sections, corner regions of CF-1 series and flat portions of CF-2 portions) could be accurately represented.

To accurately predict the structural behaviour of the modelled specimens, measured geometries and engineering stress–strain relationships for HSS HexHS were incorporated into the FE models. The measured stress–strain material properties from the flat coupons and the corner coupons as well as the weldments were converted to the true stress and logarithmic plastic strain [34]. Initial geometric imperfections are generated during transportation, fabrication, erection, storage as well as installation, which can affect the structural performance and ultimate resistance of structural members. Thus, the measured initial local geometric imperfection magnitudes from the companion experimental study [35] were incorporated into the FE models using the mode

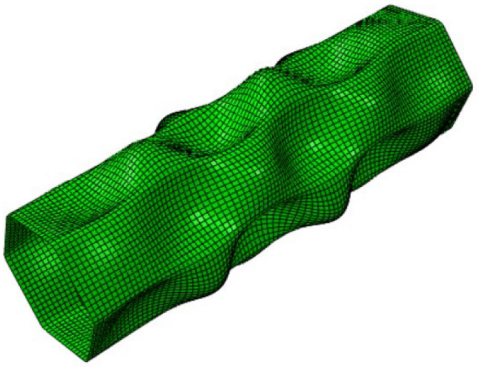

Fig. 3. Typical first buckling mode shape generated from Eigenvalue analysis.

shapes obtained from a prior linear elastic buckling analysis. The lowest elastic buckling mode under concentric compression was selected as the imperfection profile, which generally represents the most unfavourable imperfection pattern. It should be noted that distorsional buckling was observed in polygonal sections such as pentagon and heptagon [51], special attention was therefore paid to the possibility of having secondary distorsional buckling or local-distortional interaction [52]. The HSS HexHS examined in this study are doubly symmetric sections in the closed form, which experience the local buckling with no sections failed in distorsional buckling or local-distortional interaction mode. The measured initial local geometric imperfection magnitudes were scaled to the corresponding imperfection profile from linear perturbation analysis, as shown in Fig. 3.

The boundary conditions were simulated in accordance with the experimental set-up for testing the HSS HexHS structures, as shown in Fig. 4. Each end cross-section was connected to the reference point locating at the centroidal point through kinematic coupling constraints. The reference points on two sides were restrained against all the degrees of freedom, except for the axial translation at the loaded end where the compressive load was applied using a static RIKS step. The geometric nonlinearity was enabled to allow for large displacement analysis by activating the option of (*NLGEOM). It should be noted that special attention was paid to the modelling of stocky sections with the failure mode in elephant foot buckling. It was observed that the circumferential expansion occurred near the end section of the stocky specimens due to the Poisson effect. To capture the failure mode and load–displacement curve response accurately and consistently, the in-plane translations at the end of these stocky sections were not restrained in accordance with the guidelines given in [53] to model elephant foot buckling at one end.

The inter-lock residual stresses induced by press-braking and welding procedures exist in the initial state, prior to the application of external loading. The residual stresses comprise bending residual stresses and membrane residual stresses. To accurately capture and predict the structural behaviour, the effect of residual stresses should be explicitly considered. The tensile coupon specimens featured with curved shapes due to the release of bending residual stresses in the process of specimen extraction from the cross-sections of HexHS. The effect of bending residual stresses was therefore inherently introduced in the measured stress–strain curves during the straightening of specimens in tensile coupon tests [34,41]. Hence, only the membrane residual stresses were incorporated into the FE modelling of HSS HexHS accounting for the effect of residual stresses. The characteristics of the membrane and bending residual stresses of HSS HexHS with different fabrication routes were measured and reported in [34] with predictive model proposed. The effect of the residual stresses was thereafter incorporated into the FE models using the magnitudes determined from the predictive model, as shown in Fig. 5.

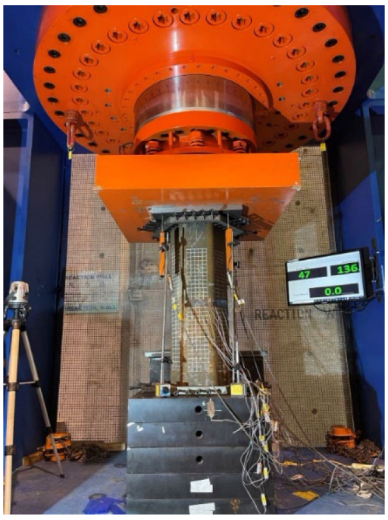

Fig. 4. Experimental set-up for testing HSS HexHS stub columns under pure compression with a specimen in place.

Typical initial stress distribution after incorporating the membrane residual stresses in the FE model with various fabrication routes are depicted in Fig. 6, with positive values indicating tensile membrane residual stress and negative values indicating compressive membrane residual stress. For instance, the largest membrane residual stress was found at the welding regions with a magnitude of $0.35f_{y,p}$ where $f_{y,p}$ refers to the yield strength of the parent plate, as shown in Fig. 6.

The enhanced material properties at the corner regions due to the cold-forming effect should be explicitly taken into account in FE models for accurate structural analysis. Therefore, the increased material strengths were incorporated by assigning the measured stress–strain relationships to the corner portions of the FE models. Previous experimental investigations found that the strength enhancements were not only limited to the corner portion, and may be also extended to the regions at a distance away from the cold-bent corners. A sensitivity study was therefore performed to investigate the effect of the extension of the corner region in this study for cold-formed sections while no corner extension was applied to the welded sections. The sections without corner extension of strength enhancements yield comparable and close predictions in terms of normalised ultimate resistance as those with corner extensions of t and $1.5t$, as shown in Table 1. The mean value of the normalised resistance between numerical value to the tested one $N_{u,FE}$ / $N_{u,test}$ is equal to 0.98 with coefficient of variation CoV = 0.028. Hence, the improved strength was assigned to the corresponding corner portion only without further extension in this study.

2.3. Validation of the FE models

The FE models were validated by comparing the numerically obtained ultimate resistance, load-end shortening relationships, and failure modes with those obtained from the experimental results. Apart from the measured initial local geometric imperfections, imperfection sensitivity studies were carried out to determine a proper magnitude of initial imperfection to be incorporated to the FE models. Four initial imperfection magnitudes, including (i) the measured imperfection value ω_o and the remaining three magnitudes, expressing in a form of the fraction to the plate thickness, (ii) $t/100$ (iii) $t/50$ (iv) $t/10$, were assessed and compared [54]. The ultimate resistances obtained from the FE models were normalised to those derived from experimental tests with varying imperfection magnitudes and are reported in Table 1. Mean values of the nomalised ratios of $N_{u,FE}/N_{u,test}$ for the four investigated initial local imperfection magnitudes are 0.98, 1.01, 1.01 and 0.98 respectively with corresponding CoVs of 0.025, 0.026, 0.025

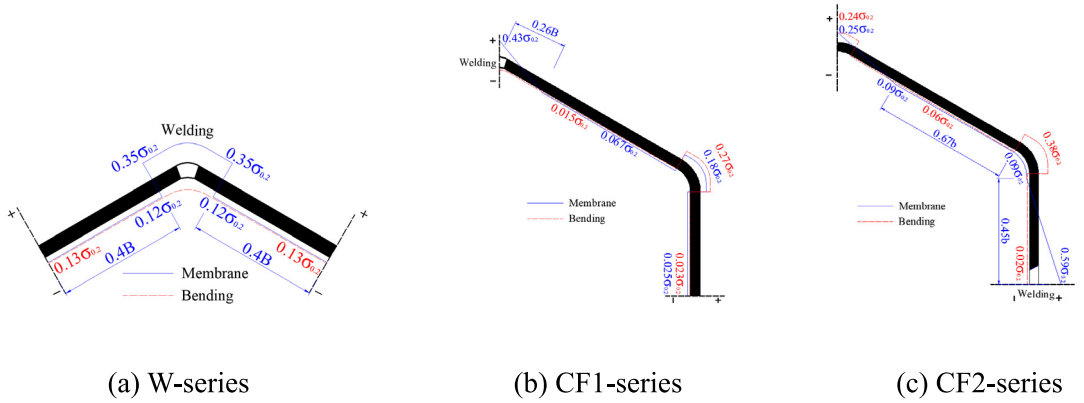

Fig. 5. Predictive models of membrane and bending residual stresses distributions and amplitudes (in MPa) for HSS HexHS stub columns [34].

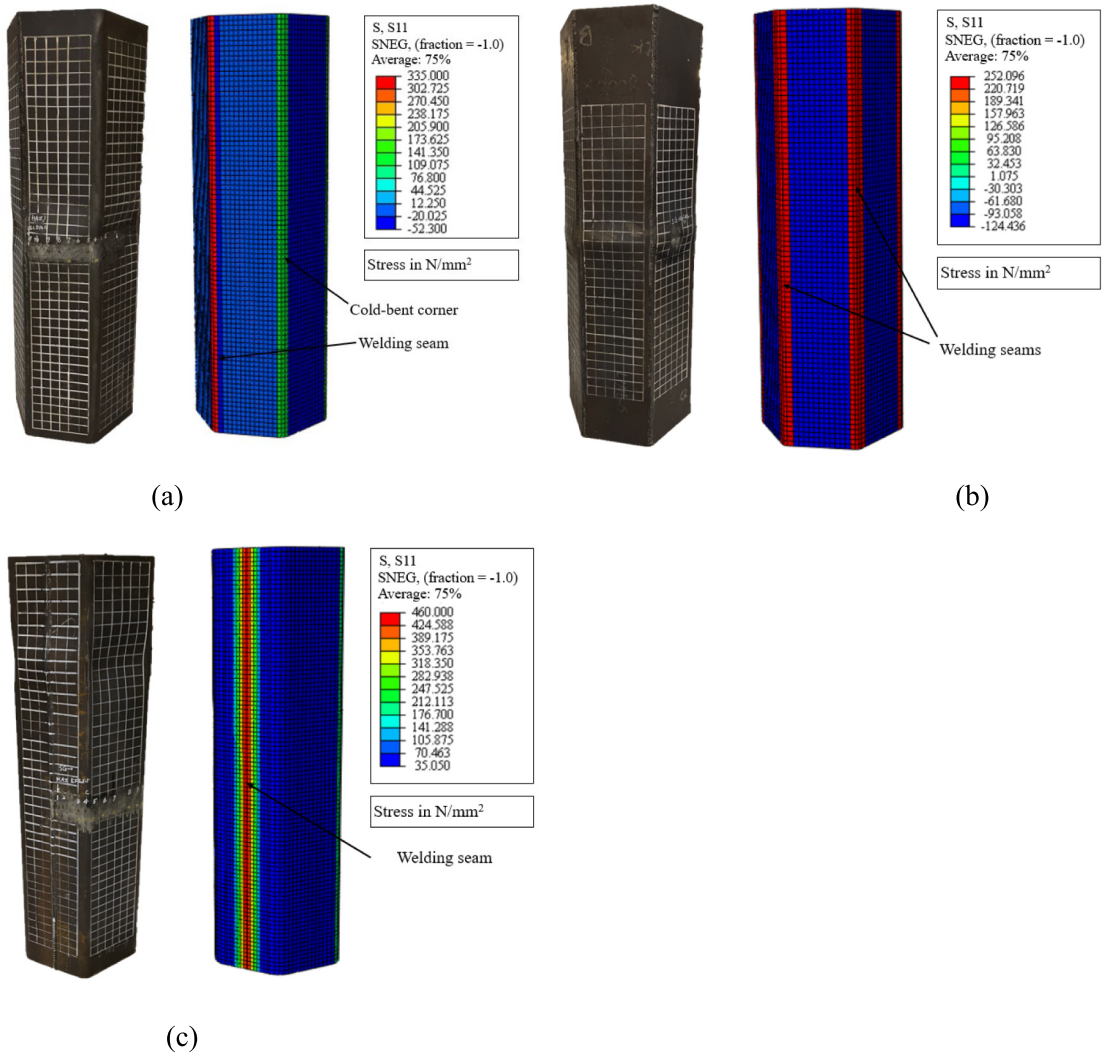

Fig. 6. Typical membrane residual stress distributions in the modelled HSS HexHS stub columns of (a) HEX-150 × 6-W (b) HEX-150 × 6-CF1 (c) HEX-150 × 6-CF2.

and 0.025 respectively. It should be noted that the relatively lower differences of the normalised ratios (1% difference) are obtained using initial imperfection values equal to $t/100$ and $t/50$, the predictions of cross-sectional resistances are somewhat on unconservative side, as shown in Table 1. Although the predictions using initial imperfection value of $t/10$ leads to slightly higher difference (2% difference) than the above mentioned two imperfection values, the cross-section resistances are located on safe side with appropriate conservatism, and the predictions are comparable and consistent with the predicted results with the measured imperfection values. The necessities for the incorporation of residual stresses into the FE models were assessed by comparing the ultimate resistance as well as the axial load-end shortening relationships from FE models with or without inclusion of residual stresses to the experimentally tested results [28,55]. The

Table 1
Comparison of the experimental and numerical results.

Specimen	$N_{u,FE}$ / $N_{u,test}$					$N_{u,FE}$ / $N_{u,test}$			$N_{u,FE}$ / $N_{u,test}$	
	Imperfection amplitudes					Corner extension (imp[b] = ω_0)			Membrane residual stress	
	ω_0		$t/100$	$t/50$	$t/10$	Without	Extended to t	Extended to $1.5t$	With (imp[b] = ω_0)	Without (imp[b] = ω_0)
HEX-70 × 6-W	0.99		1.03	1.03	0.99	0.99	N.A.[a]	N.A.[a]	0.99	1.01
HEX-70 × 6-CF1	0.99		1.02	1.02	0.99	0.99	1.01	1.01	0.99	1.00
HEX-70 × 6-CF2	1.01		1.03	1.03	1.01	1.01	1.03	1.03	1.01	1.02
HEX-70 × 6-CF2#	1.01		1.03	1.03	1.01	1.01	1.03	1.03	1.01	1.02
HEX-150 × 6-W	0.98		1.00	1.00	0.98	0.98	N.A.[a]	N.A.[a]	0.98	1.01
HEX-150 × 6-CF1	0.95		0.97	0.97	0.95	0.95	0.97	0.97	0.95	0.96
HEX-150 × 6-CF2	0.96		0.98	0.98	0.96	0.96	0.97	0.97	0.96	0.98
HEX-150 × 6-CF2#	0.96		0.98	0.98	0.96	0.96	0.97	0.97	0.96	0.98
HEX-200 × 6-W	1.00		0.98	0.98	1.00	1.00	N.A.[a]	N.A.[a]	1.00	1.05
HEX-200 × 6-CF1	1.05		1.03	1.03	1.05	1.05	1.05	1.05	1.05	1.05
HEX-200 × 6-CF2	0.97		0.95	0.95	0.97	0.97	0.97	0.97	0.97	0.97
HEX-155 × 10-W	0.97		1.02	1.01	0.97	0.97	N.A.[a]	N.A.[a]	0.97	0.99
HEX-155 × 10-CF1	0.97		1.02	1.01	0.97	0.97	0.98	0.98	0.97	0.99
HEX-155 × 10-CF2	0.97		1.01	1.01	0.97	0.97	0.98	0.98	0.97	0.99
HEX-155 × 10-CF2#	0.97		1.01	1.01	0.97	0.97	N.A.[a]	N.A.[a]	0.97	0.99
HEX-185 × 10-W	1.01		1.05	1.04	1.01	1.01	1.03	1.03	1.01	1.00
HEX-185 × 10-CF1	1.00		1.03	1.03	1.00	1.00	1.01	1.01	1.00	1.02
HEX-185 × 10-CF2	0.96		0.99	0.99	0.96	0.96	0.97	0.97	0.96	0.98
	Mean	0.98	1.01	1.01	0.98	0.98	0.99	0.99	0.98	1.00
	CoV	0.025	0.026	0.025	0.025	0.028	0.027	0.027	0.025	0.024

Note:
[a]Indicates that corner extension is not applicable to welded sections W-series.
[b]Indicates initial local geometric imperfection magnitude.

Table 2
Key material properties adopted in parametric study.

Steel grade	Flat portion				Corner portion			
	E_f (N/mm^2)	$f_{y,f}$ (N/mm^2)	$f_{u,f}$ (N/mm^2)	$\varepsilon_{u,f}$ (%)	E_c (N/mm^2)	$f_{y,c}$ (N/mm^2)	$f_{u,c}$ (N/mm^2)	$\varepsilon_{u,c}$ (%)
Q460 [56]	213 900	581	669	11.7	198 200	735	776	1.33
Q690 [34]	210 000	770	825	6.5	200 000	815	845	1.75

minimal difference within 2% was found in the ultimate resistance and axial load-end shortening curves were almost identical for cold-formed HSS HexHS (CF-1 series and CF-2 series), indicating the inclusion of membrane residual stress is unnecessary for cold-formed sections due to its negligible effect on the structural response, as seen in Table 1. However, residual stresses affect the stub column behaviour of welded sections (W-series) within 4% differences in terms of the ultimate load, leading to somewhat premature yielding and increasing the deformation capacity at moderate level. Hence, the membrane residual stresses were thereafter taken into account in welded HSS HexHS rather than cold-formed HSS HexHS. The graphical comparison of the axial load-end shortening curves is shown in Fig. 7, demonstrating the minimal effect of membrane residual stresses for cold-formed HSS HexHS stub columns.

The comparison shown in Fig. 7 also underlines that membrane residual stresses have relatively larger effect on slender sections than stocky sections, principally due to the fact that the stress can be redistributed within the cross-sections after entering plasticity within the stocky sections whereas for slender sections the superimposition of the residual stresses with stress induced by external loads simply leads to local buckling prior to the yield load without stress redistribution [57]. Overall, initial stiffness and load-end shortening curves between FE modelling and test results correlate well with each other. The ultimate resistances determined from the FE models closely match those obtained from experimental results and the failure modes from the FE models mirrored those observed in physical experiments, as shown in Fig. 8. It is therefore concluded that the developed FE models are able to produce accurate and consistent predictions of the tested HSS HexHS and suitable for performing the subsequent parametric studies.

2.4. Parametric study

Based upon the validated FE models, an extensive parametric study was conducted on HSS HexHS to expand the available tested results over a wider spectrum of geometries and cross-section slenderness to investigate the applicability and accuracy of the existing design codes and design approaches. It should be noted that no existing stress–strain properties for hexagonal hollow sections with nominal yield strength of 460 MPa can be found. The experimental investigations on material properties reported in Liu et al. [36] imply that the effect of the cold-bent angle on material properties and residual stresses is minimal. Hence, the material properties of OctHS with 135 degrees cold-bent corners are considered to be applicable to HexHS with cold-bent corner of 120 degrees on conservative side. The full stress–strain curves for steel grades of Q460, Q690 with nominal yield strength equal to 460 MPa and 690 MPa reported in Chen et al. [56] and Liu et al. [34] were used.

The average material properties from measurements were used with key material properties adopted in parametric study for both flat and corner portions, as reported in Table 2 which includes Young's modulus E, the yield strength f_y, the ultimate strength f_u, and the ultimate strain ε_u. The letters of "f" and "c" in subscript denote the flat and corner portions of the cross-sections. The stress–strain relationships with nominal yield strength of 460 MPa and 690 MPa were re-constructed using the proposed predictive stress–strain models given in [34,56] and are plotted in Fig. 9. For cold-formed CF-1- and CF-2 series, increased material properties were assigned to the corner regions, and flat materials were employed for flat portions only for all series specimens, whereas material properties of the weldments were assigned to the corresponding butt welding for W-series sections. The

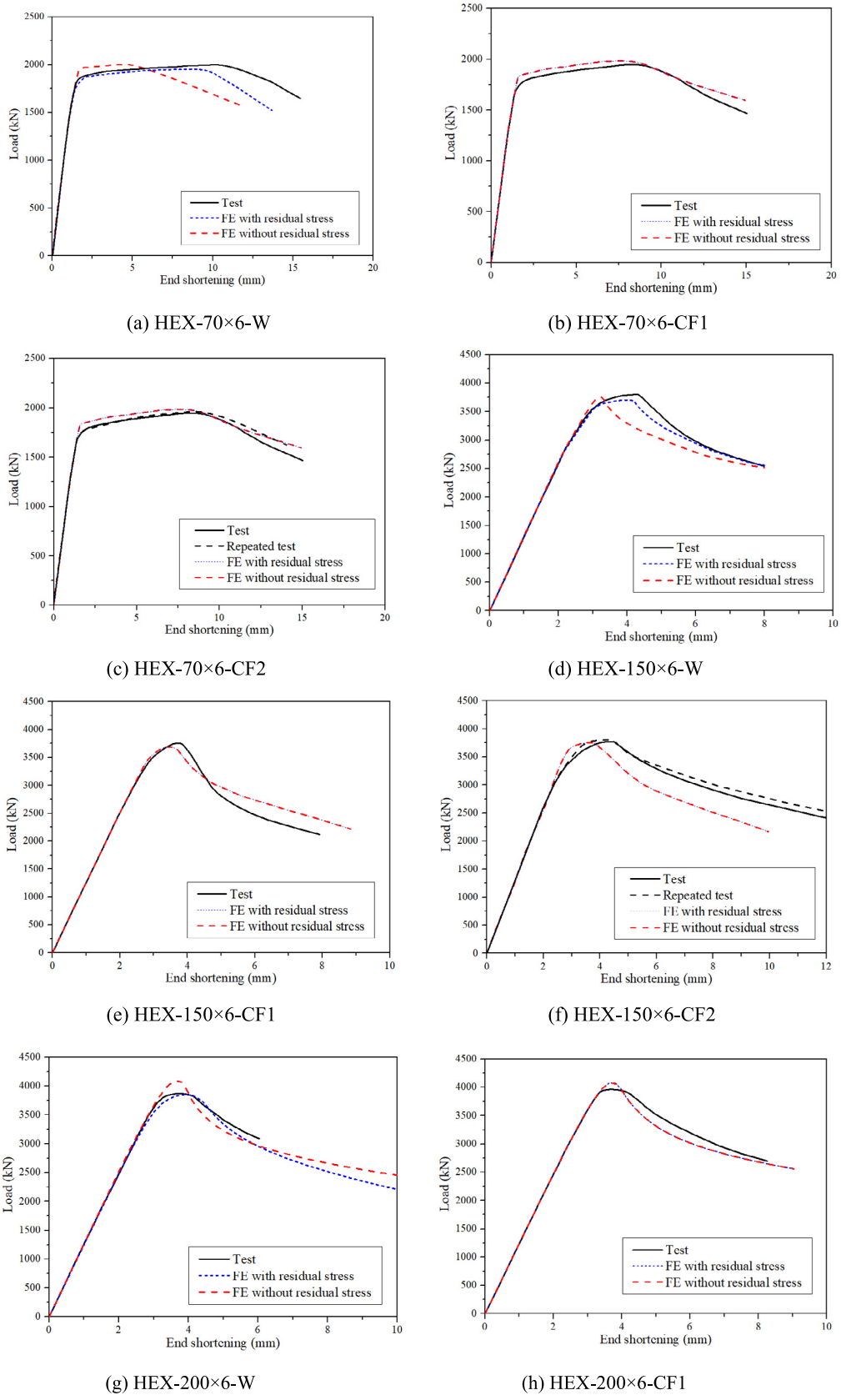

Fig. 7. Comparison of load-end shortening curves of HSS HexHS stub columns between experimental and numerical results.

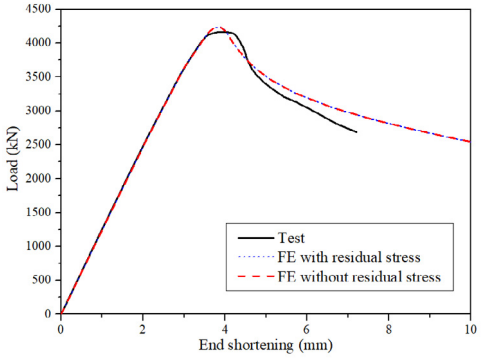

(i) HEX-200×6-CF2

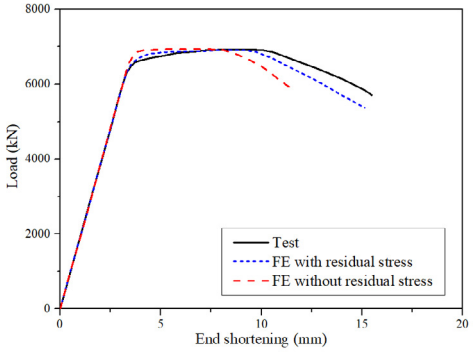

(j) HEX-155×10-W

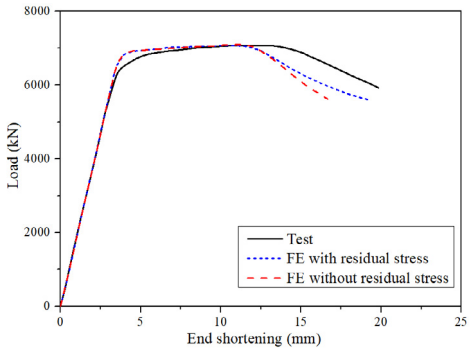

(k) HEX-155×10-CF1

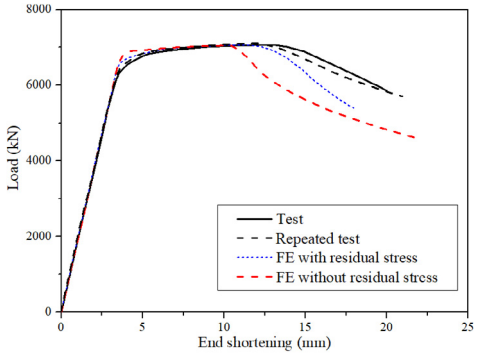

(l) HEX-155×10-CF2

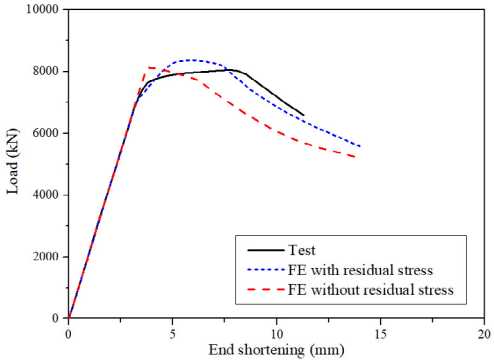

(m) HEX-185×10-W

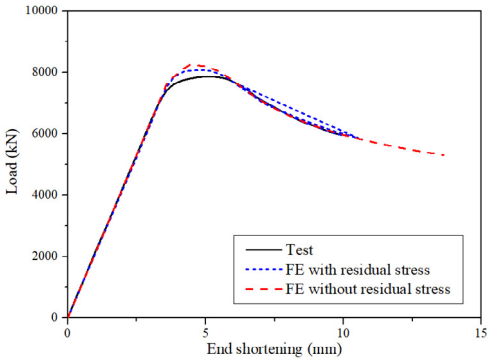

(n) HEX-185×10-CF1

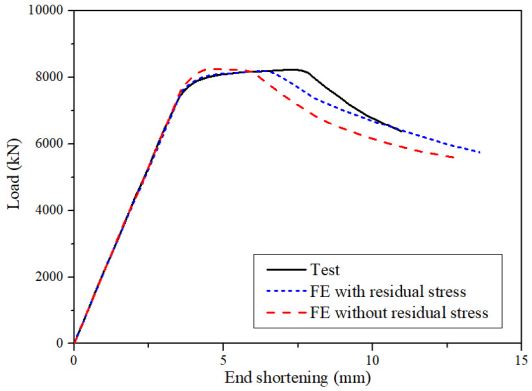

(o) HEX-185×10-CF2

Fig. 7. (*continued*).

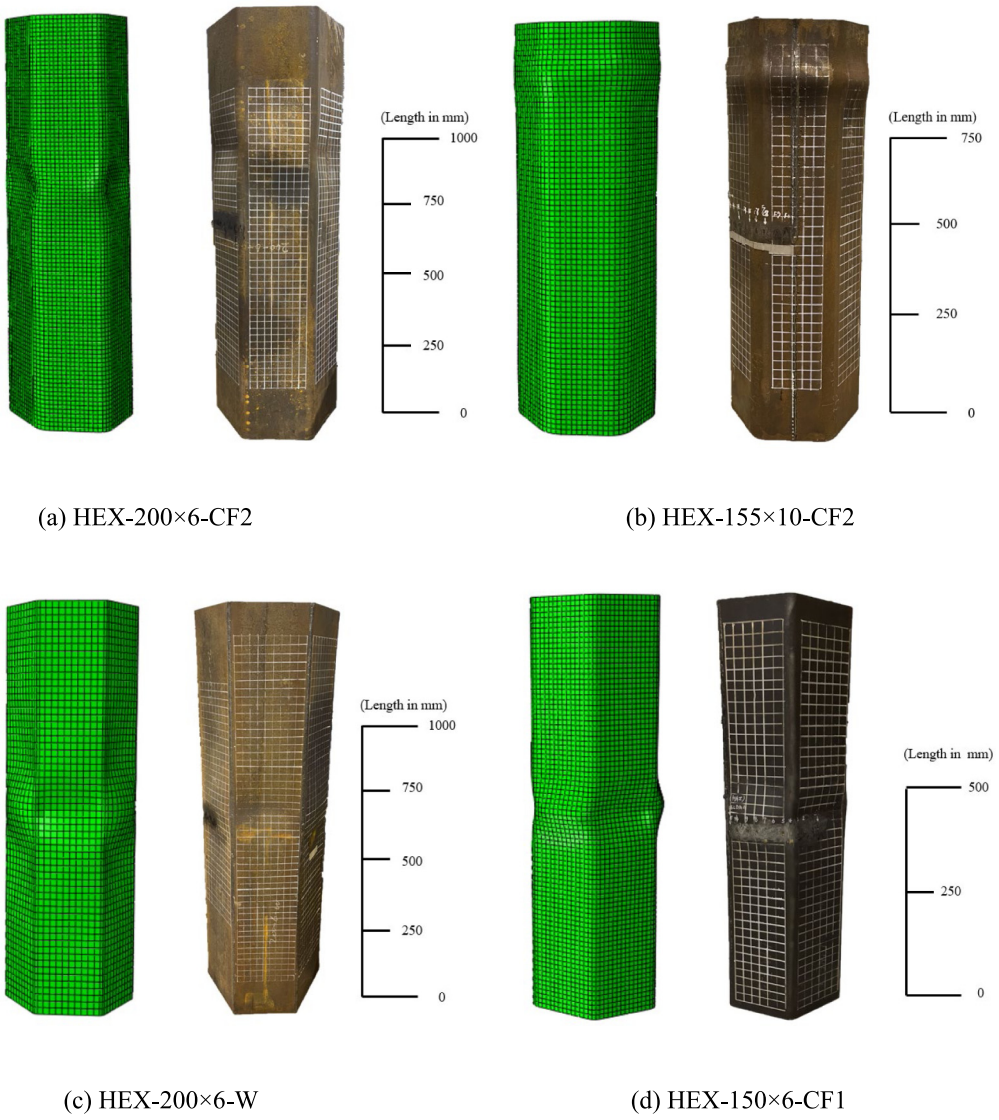

Fig. 8. Comparison of the test and FE failure modes for typical stub column specimens.

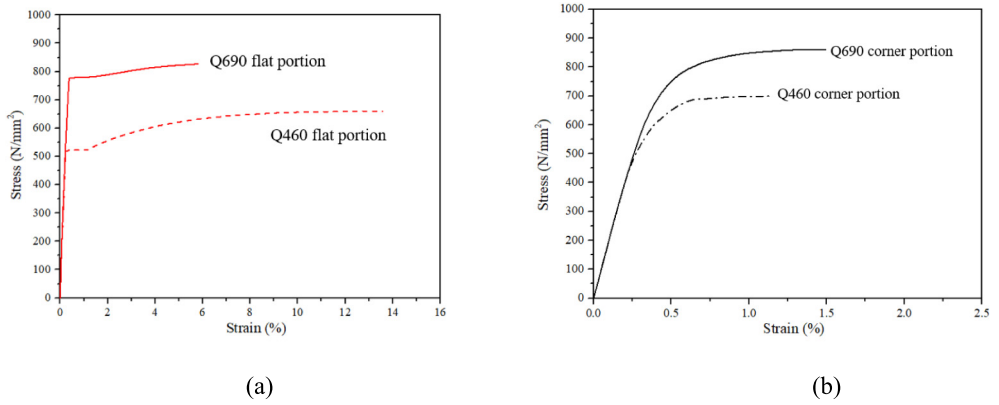

Fig. 9. Stress–strain curves of employed in parametric study for HexHS (a) Stress–strain curves of flat portions (b) Stress–strain curves of corner portions.

investigations carried out in Chen et al. [58] and Schaper et al. [59] demonstrated that there is no clear tendency depending on the steel grade for residual stress magnitude, thus the residual stress distribution for HSS HexHS was also applied to FE models with lower yield strength of 460 MPa, which was deemed to be on a safe-sided consideration. The length of all the specimens was designed as 2.5 times the largest plate width, which was deemed to be short enough to avoid the occurrence of global buckling but sufficiently long to contain the representative initial local geometric imperfection and residual stresses. The thickness of the modelled HexHS was kept constant as 6 mm to avoid the variations

Table 3
Summary of the cross-section yield slenderness limits in design codes and design approaches.

Design standards and methods	Yield slenderness limits	λ_{lim} [a]
EN 1993-1-1	$b/t \leqslant 42\varepsilon_{EC3}$, $\varepsilon_{EC3} = \sqrt{235/f_y}$, $E = 210$ GPa	1.405
ANSI/AISC 360-16	$b/t \leqslant 1.40\varepsilon_{AISC}$, $\varepsilon_{AISC} = \sqrt{E/f_y}$, $E = 200$ GPa	1.400
EN 1993-1-5	$\overline{\lambda_p} = \frac{b/t}{28.4\varepsilon\sqrt{k}} \leq 0.5 + \sqrt{0.085 - 0.055\psi}, \psi = 1, \varepsilon_{EC3} = \sqrt{235/f_y}, k_\sigma = 4, E = 210$ GPa	1.279
AS 4100	$b/t \leqslant \xi^{b}\varepsilon_{AS4100}$, $\varepsilon_{AS4100} = \sqrt{250/f_y}$, $E = 200$ GPa	1.414
ASCE/SEI 48-11	$b/t \leqslant 681.2/\sqrt{f_y}$, $E = 200$ GPa	1.520
DSM	$\lambda_p = \sqrt{f_y/f_{cr}} \leq 0.776$, $E = 200$ GPa	1.470
CSM	$\lambda_p = \sqrt{f_y/f_{cr}} \leq 0.68$, $E = 200$ GPa	1.290

Note:
[a] λ_{lim} is equal to $(b/t)(f_y/E)^{0.5}$ which is specified in AISC 360-16. This form was adopted as the standard expression to harmonise the various forms of slenderness limits expressions from other design codes.
[b] indicates the parameter to account for the effect of welding with $\xi = 40$ for cold-formed and light welded sections and $\xi = 35$ for heavily welded sections.

between the yield strength and the plate thickness, and the inner corner radius of the cold-bent corner of each specimen r_i was taken equal to three times of its nominal thickness for cold-formed section series to avoid cracking subject to larger plastic deformation caused by press-braking. In terms of the geometries, the clear width of the flat portion b was varied from 20 mm to 330 mm for sections with aspect ratio of 1.0. A total of 1440 FE models were modelled in the parametric studies.

3. Evaluation of existing design codes and design approaches

3.1. General

At present, there are no design specifications for HSS HexHS in structural steel design codes such as the Eurocode 3 (EC3), including EN 1993-1-1 [45], EN 1993-1-5 [48], EN 1993-1-12 [47], American code of ANSI/AISC 360-16 [43], Australian code of AS 4100 [44] as well as the design code of transmission pole structures of ASCE/SEI 48-11 [46]. Hence, the applicability and accuracy of the existing design codes were assessed for HSS HexHS under axial compression. In addition to the design codes, the recently proposed design approaches of Direct Strength Method (DSM) and Continuous Strength Method (CSM) were also considered, and their applicability were discussed.

3.2. Cross-section classification

In the framework of the European code of Eurocode 3 [45,47], the American design code of ANSI/AISC 360-16 [43] and the Australian code of AS 4100 [44], the concept of cross-section classification is adopted to distinguish the cross-sectional behaviour. The sections under concentric compression, which can attain the yield load without local buckling are denoted as Class 1–3 sections while Class 4 sections are those that fail by local buckling prior to the attainment of yield load. AISC 360-16 [43] and AS 4100 [44] use the terms slender and non-slender sections to classify the cross-sectional behaviours, that slender section and non-slender sections are equal to Class 4 and Class 1–3 sections respectively. The cross-section slenderness based on the plate width-to-thickness ratios or diameter-to-thickness ratios is used as a governing parameter for cross section classification under concentric compression. It should be noted that the design code for steel transmission pole ASCE/SEI 48 [46] stipulates the guidance on hexagonal hollow sections, thus the slenderness limits provided in ASCE/SEI 48 [46] were also assessed. For simple and direct purposes, the form of slenderness limit value $\lambda_{lim} = (b/t)(f_y/E)^{0.5}$ specified in AISC 360-16 [43] was adopted as the standard expression to harmonise the various forms of slenderness limits expressions from other design codes.

In conjunction with the comparison with design codes, advanced design approaches of DSM and CSM were also compared. Design process of DSM and CSM is also briefly introduced in this paragraph. There is no cross-section shape limitation for DSM as the constituent plate interaction within arbitrary cross-section shape can be inherently accounted for in its overall cross-section slenderness $\lambda_p = (f_y/f_{cr})^{0.5}$, where f_y is the yield strength of the steel material and f_{cr} is the critical elastic buckling stress determined in accordance with CUFSM [60] program using the finite strip method. Due to the closed section nature of tubular sections and the relatively short member length, neither global buckling nor distorsional buckling was observed. The nominal axial strength predicted by DSM was thereby taken as the nominal strength of local buckling. Different from DSM, the CSM is a deformation-based design method, which can take strain hardening and effect of element interaction into consideration. The iteration of the effective area of the cross section due to local buckling and cross-section classification is not needed in the design strength predictions, this method was also evaluated for its application to HSS HexHS in this study. Note also that the expression of cross-section slenderness limit used by CSM is exactly the same as the one used in DSM. DSM specifies that cross-section with slenderness limit λ_p greater than 0.77 cannot reach the yield load, whereas limit value of 0.68 is provided by CSM. A summary of the yield slenderness is tabulated in Table 3.

3.3. Cross-section resistance

In design framework of Eurocode 3, structural components failed by local buckling before attaining the yield load are considered to resist the external loading with the effective width b_{eff}, whereupon the resultant cross-sectional resistance is equal to $A_{eff}f_y$. The A_{eff} is the effective area of the section. The methodology of the effective width method (EWM) is also adopted in design codes of AISC 360-16 and AS 4100, though the expressions are different. The material related parameters of $\varepsilon_{EC3} = (235/f_y)^{0.5}$, $\varepsilon_{AISC} = (E/f_y)^{0.5}$, and $\varepsilon_{AS4100} = (250/f_y)^{0.5}$ are used in these three codes respectively to consider the impact of material strength. The effective width method and formulae given in EN 1993-1-5 are as follows in Eq. (1). The reduction of the original width b to the effective width b_{eff} of the slender plate elements is dependent on the boundary conditions, stress gradients, and dimensions.

$$\frac{b_{eff,EC3}}{b} = \begin{cases} 1 & \text{for } \overline{\lambda}_p \leq 0.5 + \sqrt{0.085 - 0.055\psi} \\ \dfrac{\overline{\lambda}_p - 0.055(3+\psi)}{\overline{\lambda}_p{}^2} & \text{for } \overline{\lambda}_p > 0.5 + \sqrt{0.085 - 0.055\psi} \end{cases} \quad (1)$$

where $\overline{\lambda}_p$ is the plate slenderness specified in EN 1993-1-5 [48], with the expression shown in Table 3. In the equation for $\overline{\lambda}_p$, k_σ is the buckling factor taken as 4 for internal plate element in compression, and ψ is the stress distribution factor with $\psi = 1$ for elements under pure compression.

In American Specification of ANSI/AISC 360-16 [43], the limiting width-to-thickness ratio is specified as the governing design limits.

Cross-sections with width-to-thickness ratios larger than the limiting values are considered to be slender sections. The relationship between original width b and effective width $b_{\mathrm{eff,AISC}}$ in AISC 360-16 is given in Eqs. (2)–(4).

$$\frac{b_{\mathrm{eff,AISC}}}{b}=\begin{cases}1 & \text{for } b/t \le \lambda_{\mathrm{r}}\sqrt{\dfrac{F_y}{F_{\mathrm{cr}}}}\\ (1-c_1\sqrt{\dfrac{F_{\mathrm{el}}}{F_{\mathrm{cr}}}})\sqrt{\dfrac{F_{\mathrm{el}}}{F_{\mathrm{cr}}}} & \text{for } b/t > \lambda_{\mathrm{r}}\sqrt{\dfrac{F_y}{F_{\mathrm{cr}}}}\end{cases} \tag{2}$$

$$F_{\mathrm{el}}=(c_2\frac{\lambda_{\mathrm{r}}}{b/t})^2F_{\mathrm{y}} \tag{3}$$

$$c_2=\frac{1-\sqrt{1-4c_1}}{2c_1} \tag{4}$$

where λ_{r} is the limiting width-to-thickness ratio of the plate, F_{el} is the elastic local buckling stress of the uniform compression plate element, c_1 and c_2 are the effective width imperfection adjustment factors. For the cold-formed HexHS sections, the $c_1 = 0.20$ and $c_2 = 1.38$ for walls of square and rectangular hollow sections were used. F_{cr} is the critical stress of the compression members with non-slender element sections which can be determined following Eq. (5).

$$F_{\mathrm{cr}}=\begin{cases}(0.658^{\frac{F_y}{F_e}})F_{\mathrm{y}} & \text{for } KL/\mathrm{r} \le 4.71\sqrt{\dfrac{E}{F_y}}\\ 0.877F_{\mathrm{e}} & \text{for } KL/\mathrm{r} > 4.71\sqrt{\dfrac{E}{F_y}}\end{cases} \tag{5}$$

where K is the effective length factor, L is the member length, r is the radius of gyration about the bending axis, E is the elastic modulus of steel, F_{e} is the elastic critical stress of the compression member, $F_{\mathrm{e}} = \pi^2E/(KL/r)^2$. Rearranging the above formulae, the design equation of effective width can be derived in a form of limiting width to thickness ratio as shown in Eq. (6).

$$\frac{b_{\mathrm{eff,AISC}}}{b}=\frac{1.38\lambda_{\mathrm{p,AISC}}}{\lambda}-\frac{0.38{\lambda_{\mathrm{p,AISC}}}^2}{\lambda^2} \tag{6}$$

In terms of Australian code of AS 4100 [44], the original width is reduced to effective width of b_{AS4100}, as shown in Eq. (7).

$$\frac{b_{\mathrm{eff,AS4100}}}{b}=\frac{\xi}{b/(t\varepsilon_{\mathrm{AS4100}})} \tag{7}$$

where ξ is the parameter to account for the effect of welding that $\xi = 40$ for cold-formed and light welded sections and $\xi = 35$ for heavily welded sections. In accordance with AS 4100 [44], heavily welded sections refer to those sections with compressive residual stress larger than 40 MPa. Therefore, the cross-sectional resistances for W-series and CF-1 series and CF-2 series are determined accordingly.

Design code of transmission pole structures ASCE/SEI 48-11 [46] which stipulates the design provisions concerning HexHS was also evaluated, as shown in Eq. (8).

$$f_{\mathrm{a,ASCE}}=\begin{cases}f_{\mathrm{y}} & \text{for } \dfrac{b}{t} \le \dfrac{681.2}{\sqrt{f_{\mathrm{y}}}}\\ 1.42f_{\mathrm{y}}(1-\dfrac{0.00114}{2.62}\dfrac{b\sqrt{f_{\mathrm{y}}}}{t}) & \text{for } \dfrac{681.2}{\sqrt{f_{\mathrm{y}}}} \le \dfrac{b}{t} \le \dfrac{919.6}{\sqrt{f_{\mathrm{y}}}}\\ 4\dfrac{\pi^2E}{12(1-\nu^2)}(\dfrac{t}{b})^2 & \text{for } \dfrac{919.6}{\sqrt{f_{\mathrm{y}}}} \le \dfrac{b}{t}\end{cases} \tag{8}$$

where A is the gross cross-section area, $f_{\mathrm{a,ASCE}}$ is the effective compressive strength, f_{y} is the yield strength and b is the clear side width excluding corner portion.

For design approach of DSM [61], repetitive calculation procedures in finding the effective area of the buckled sections are not necessary and design approaches can be applied to arbitrary cross-sectional shape without limitations in comparison with design codes for which only conventional profile can be applied. For sections with slenderness smaller than $\lambda_{\mathrm{p}} = 0.776$, the yield load can be achieved whereas for those sections with cross-section slenderness limit $\lambda_{\mathrm{p}} \ge 0.776$, the predicted strength could be determined following the equation expressed by Eq. (9).

$$N_{\mathrm{DSM}}=\begin{cases}f_{\mathrm{y}}A & \text{for } \lambda_{\mathrm{p}} \le 0.776\\ (1-\dfrac{0.15}{{\lambda_{\mathrm{p}}}^{0.8}})\dfrac{1}{{\lambda_{\mathrm{p}}}^{0.8}}f_{\mathrm{y}}A & \text{for } \lambda_{\mathrm{p}} > 0.776\end{cases} \tag{9}$$

In terms of the design approach of CSM, a continuous relationship between the section slenderness and deformation capacity was established, by which the traditional classification system was replaced [62]. The CSM was originally developed to tackle the strain hardening behaviour of stainless steel [63], and was further extended to the design of carbon steel sections for both hot-rolled sections and cold-formed sections [64,65]. Hence, the appropriateness of CSM to HSS HexHS was evaluated against the experimental and numerical results. The base curve for tubular sections of SHS/RHS made from HSS was developed and proposed in Lan et al. [66], as shown in Eq. (10).

$$\begin{cases}\dfrac{\varepsilon_{\mathrm{csm}}}{\varepsilon_{\mathrm{y}}}=\dfrac{0.294}{{\lambda_{\mathrm{p}}}^{3.174}} \le \min(15,\dfrac{C_1\varepsilon_{\mathrm{u}}}{\varepsilon_{\mathrm{y}}}) & \text{for } \lambda_{\mathrm{p}} \le 0.68\\ \dfrac{\varepsilon_{\mathrm{csm}}}{\varepsilon_{\mathrm{y}}}=(1-\dfrac{0.219}{{\lambda_{\mathrm{p}}}^{1.014}})\dfrac{1}{{\lambda_{\mathrm{p}}}^{1.014}} & \text{for } \lambda_{\mathrm{p}} > 0.68\end{cases} \tag{10}$$

where $(\varepsilon_{\mathrm{csm}}/\varepsilon_{\mathrm{y}})$ is the deformation capacity, $\varepsilon_{\mathrm{csm}}$ is the CSM limiting strain, ε_{y} is the yield strain equals to f_{y}/E. Two typical material model developed by Yun and Gardner [67] are applicable to CSM design, (i) quasi-linear model for commonly used hot-rolled steels and (ii) bi-linear model which can represents the rounded response of cold-formed steel. The material models were further improved and modified in [68] by collating extensive material data from existing literatures with new material models with associated material parameters proposed. To calculate the cross-section strength from CSM, the CSM limiting stress f_{csm} needs to be derived based on CSM strain. Hence, quad-linear material model was used for W-series sections and bi-linear model was used for cold-formed section series of CF-1 and CF-2 in this study. The predicted cross-section resistance can be determined using Eq. (11).

$$N_{\mathrm{csm}}=\begin{cases}f_{\mathrm{csm}}A & \text{for } \lambda_{\mathrm{p}} \le 0.68\\ \dfrac{\varepsilon_{\mathrm{csm}}}{\varepsilon_{\mathrm{y}}}f_{\mathrm{y}}A & \text{for } \lambda_{\mathrm{p}} > 0.68\end{cases} \tag{11}$$

3.4. Assessment of cross-section classification and resistance predictions

3.4.1. Cross-section slenderness limits

To assess the suitability of cross-sectional slenderness limits, the ultimate loads obtained from experiments and numerical modelling for the specimens were firstly normalised by the corresponding yield load Af_{y}, where f_{y} was taken as the average yield strength from the flat coupons and then plotted against the normalised plate slenderness λ_{lim} of the governing plate element as shown in Fig. 10. Based on the graphical comparisons between the experimental and numerical data and the converted cross-section yield limits, it is obvious that the normalised resistance value converges to the unity at a value (intersection with the unity) far smaller than the current codified slenderness in design codes and design approaches and the yield slenderness limits in the existing structural steel design codes are located on the unsafe side for sections with yield strengths of 460 MPa and 690 MPa. This indicates that the current yield slenderness limit specified for internal plate members in structural steel design codes as well as ASCE/SEI 48-11 cannot be simply extended to cover the design of HSS HexHS. Similarly, the converted yield slenderness from the design approaches of DSM, CSM also exhibit overly predicted cross-section classification on unsafe side. As can be observed in Fig. 11, the HSS HexHS with nominal strength of 690 MPa exhibit comparably consistent normalised values among three different fabrication routes for both slender and non-slender sections

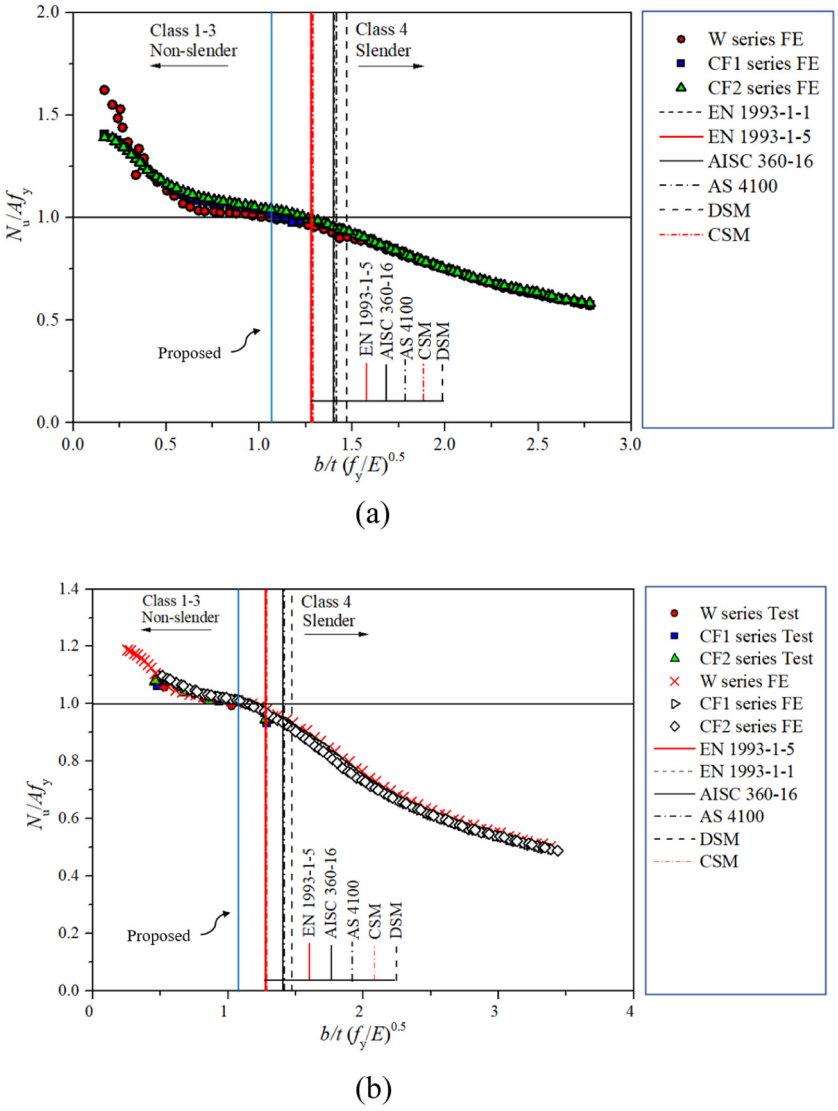

Fig. 10. Assessment of the cross-section classification yield limit from design codes and design approaches for HSS HexHS under pure compression (a) HexHS with nominal yield strength of 460 MPa (b) HexHS with nominal yield strength of 690 MPa.

whereas non-slender sections with yield strength of 460 MPa exhibit moderately different structural behaviours among three different fabrication routes with larger discrepancy. For welded-sections (W-series), the normalised cross-section resistances were lower than the cold-formed sections for stocky sections whereas the degree of disparity is decreasing with consistent normalised cross-section resistances for slender sections in all three series with different fabrication routes. For consistency and simplicity, a unified cross-section slenderness yield limit value $\overline{\lambda}_p = 0.55$ (standardised cross-section slenderness limit of $\lambda_{lim} = 1.05$) is proposed based on graphical assessment for HSS HexHS under pure compression.

3.4.2. Assessment of cross-section resistance predictions

The comparisons between design curves of the corresponding effective width equations from the design codes and the normalised values between ultimate resistances and yield load from experiments and parametric studies were made, as shown in Fig. 11. All design codes provide over-conservative predictions for the stocky sections for all investigated steel grades and sections series for different fabrication routes, as the sections are only allowed to attain the yield load without considering strain hardening effect. For slender sections, design curves from the existing design standards of EN 1993-1-5 and AISC 360-16 generally follow the decreasing tendency, whereas significant conservative predictions are provided by AS 4100. Design code of ASCE/SEI 48 shows over-conservative predictions for slender sections with slenderness λ_p larger than 1.15 and over-predicted results for sections with intermediate slenderness between 0.75 and 1.1. It is of worthy mentioning that HSS HexHS with lower strength grade were more sensitive to the membrane residual stresses than high grade, particularly for slender sections with 3% reductions in cross-sectional resistances on average.

The cross-section resistances were also assessed with the predicted values from the current design codes of Eurocode 3, ANSI/AISC 360-16, AS 4100, ASCE/SEI 48-11 as well as the predictions from the design approaches of DSM and CSM with all partial factors set to unity for direct comparison. The normalised ratios are plotted against the section slenderness in a form of $b/t\varepsilon$. In Figs. 12–15, three structural steel design codes provide relatively consistent predictions. EC3 and AISC provide relatively unsafe predictions (over-predicted) for slender sections whereas the AS 4100 yield significantly conservative results, revealing the need of developing more accurate design approaches. The largest scattered predictions are provided from ASCE/SEI 48 with either over-conservative predictions for stocky sections and slender sections or non-conservatism for specimens with intermediate slenderness values. It is observed that over-conservative predictions are provided by

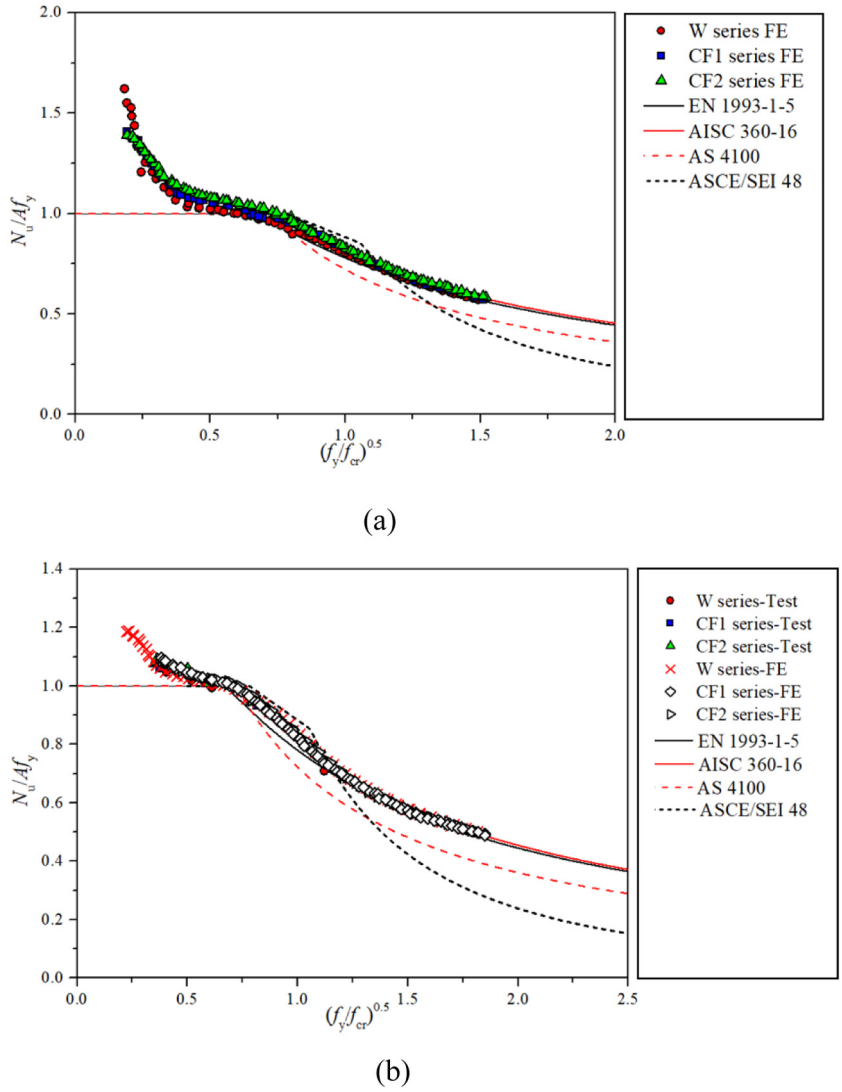

Fig. 11. Assessment of the effective width methods from design codes for HSS HexHS under pure compression (a) HexHS with nominal yield strength of 460 MPa (b) HexHS with nominal yield strength of 690 MPa.

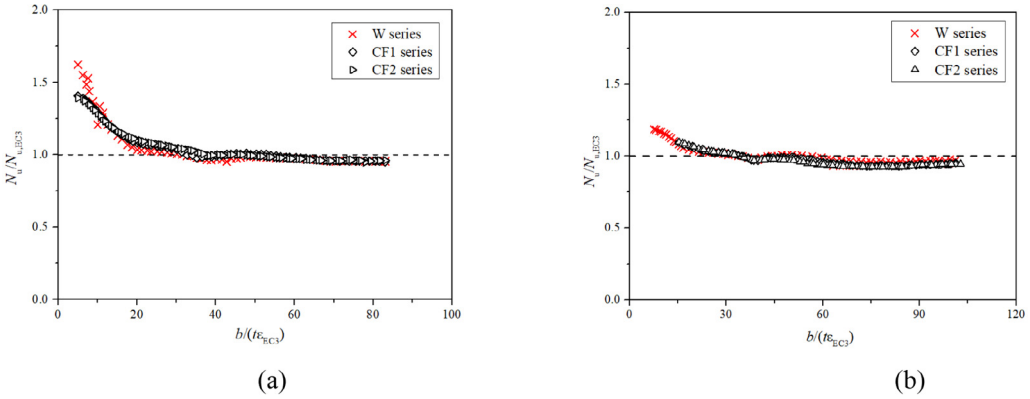

Fig. 12. Comparisons of experimental and numerical results with strength predictions from design code of Eurocode 3 for sections with nominal yield strength (a) 460 MPa (b) 690 MPa.

design codes due to the neglect of strain hardening, particularly for sections with lower strength at which the significant strain hardening are associated with, as shown in Figs. 12–15.

In terms of the comparison among design approaches, CSM generally provide more accurate predictions than DSM, which can be demonstrated in Figs. 16 and 17. The normalised resistance ratio

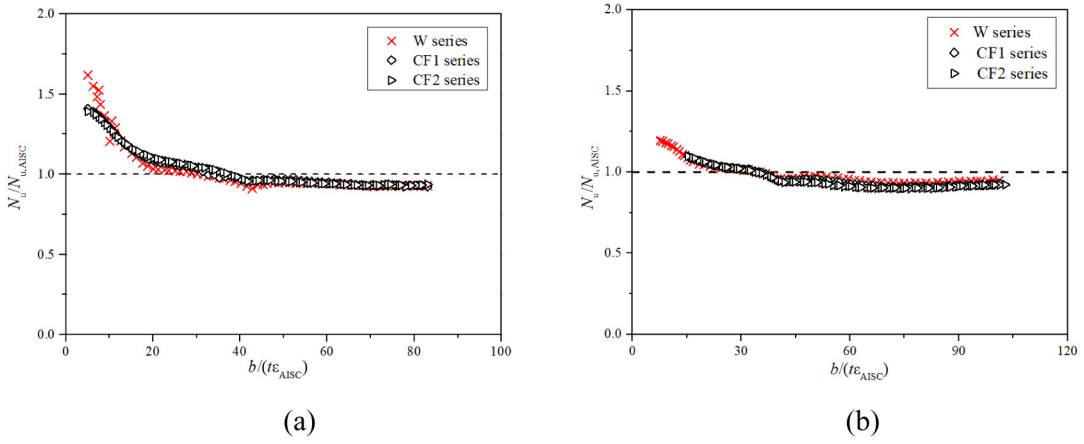

Fig. 13. Comparisons of experimental and numerical results with strength predictions from design code of AISC 360-16 for sections with nominal yield strength (a) 460 MPa (b) 690 MPa.

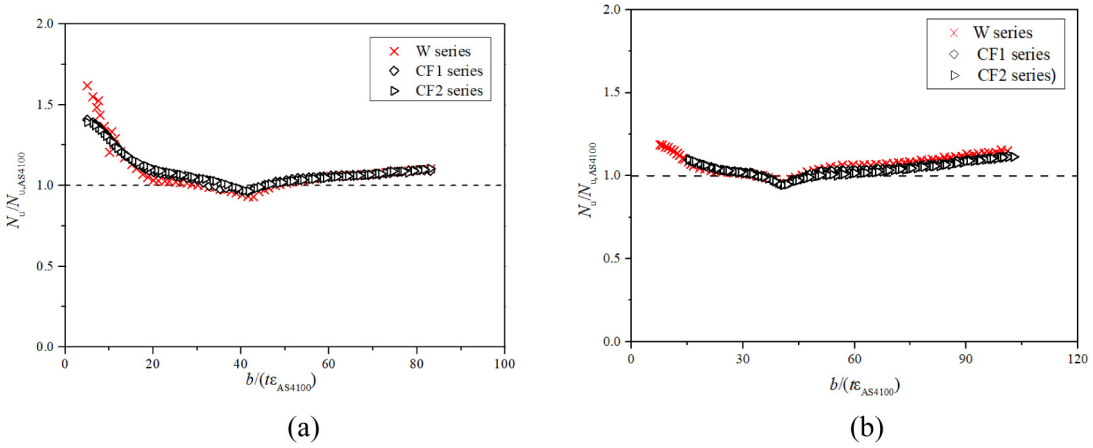

Fig. 14. Comparisons of experimental and numerical results with strength predictions from design code of AS 4100 for sections with nominal yield strength (a) 460 MPa (b) 690 MPa.

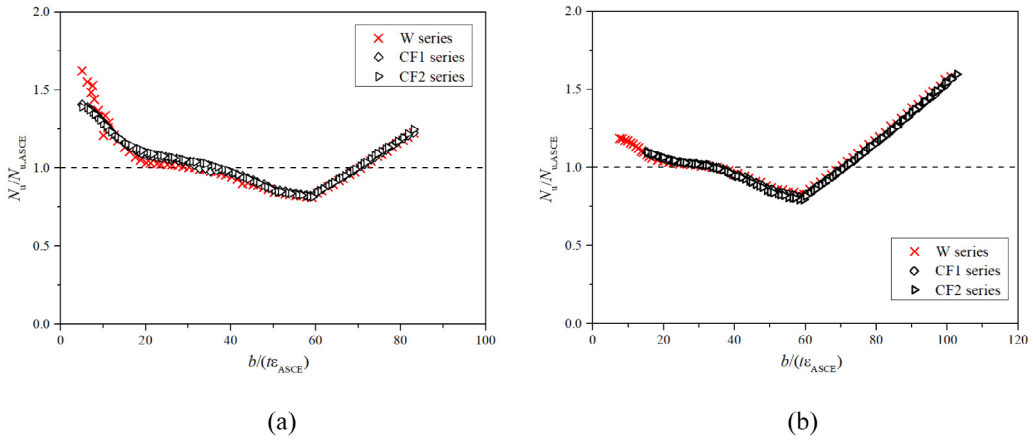

Fig. 15. Comparisons of experimental and numerical results with strength predictions from design code of ASCE/SEI 48 for sections with nominal yield strength (a) 460 MPa (b) 690 MPa.

$N_{u,test}/N_{u,pred}$ from DSM display over-predicted cross-section strength for slender sections and over conservatism for stocky sections with strain hardening. Design approach of CSM provides relatively consistent and accurate predictions as shown in Fig. 17. The mean values of ultimate strength-to-predicted ratio $N_{u,test}/N_{u,pred}$ from the design codes of Eurocode 3, ANSI/AISC 360-16, AS 4100, ASCE/SEI 48-11, and design approaches of DSM and CSM are 1.06, 1.04, 1.09, 1.05, 1.04 and 1.01 with corresponding coefficient of variations (CoVs) of 0.128, 0.139, 0.108, 0.156, 0.141 and 0.032 respectively for sections with nominal yield strength of 460 MPa. Likewise, the mean values of strength-to-predicted ratio $N_{u,test}/N_{u,pred}$ are 0.98, 0.96, 1.05, 1.07, 0.96 and 1.03 with corresponding CoVs of 0.055, 0.067, 0.046, 0.187, 0.073, and 0.018 respectively for sections with yield strength of 690 MPa. The comparison was also conducted for slender and non-slender

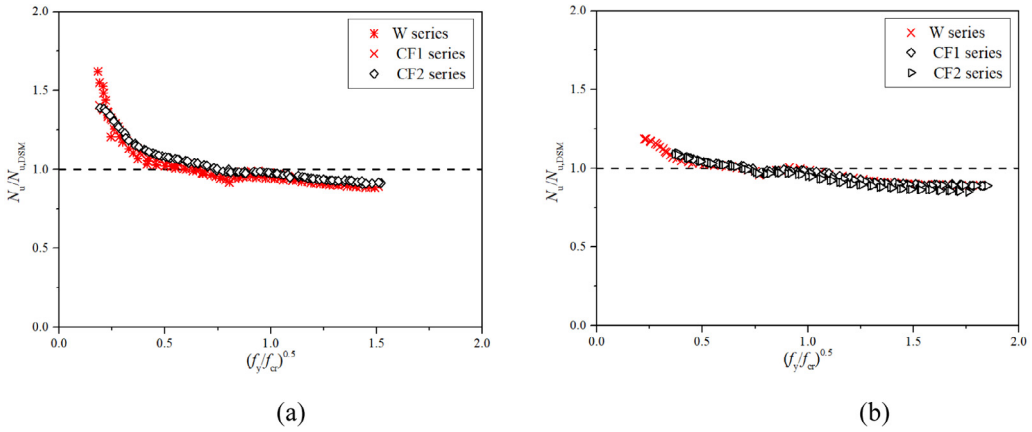

Fig. 16. Comparisons of experimental and numerical results with strength predictions from design approach of DSM for sections with nominal yield strength (a) 460 MPa (b) 690 MPa.

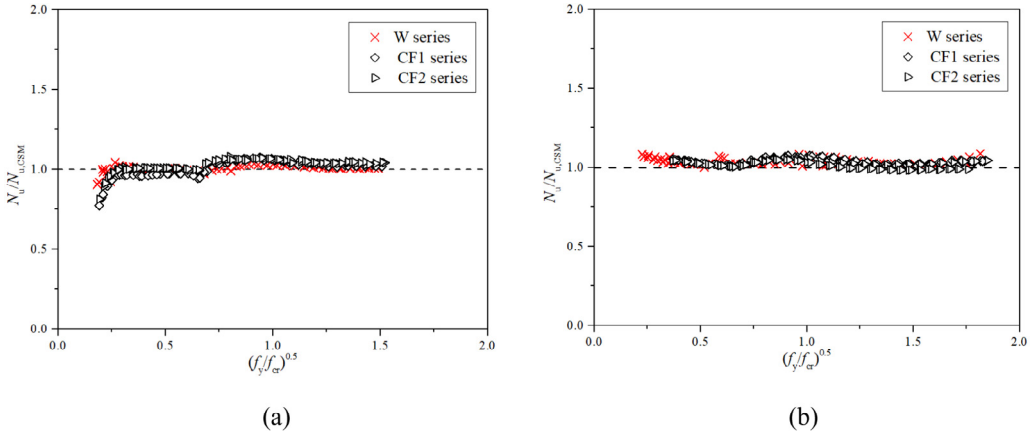

Fig. 17. Comparisons of experimental and numerical results with strength predictions from design approach of CSM for sections with nominal yield strength (a) 460 MPa (b) 690 MPa.

Table 4
Comparisons of numerical results with predicted strengths based on different design methods for HexHS with nominal yield strength of 460 MPa.

No. of specimen		$N_u/N_{u,EC3}$	$N_u/N_{u,AISC}$	$N_u/N_{u,AS4100}$	$N_u/N_{u,ASCE}$	$N_u/N_{u,DSM}$	$N_u/N_{u,CSM}$	$N_u/N_{u,EC3}{}^*$	$N_u/N_{u,DSM}{}^*$
FE:729									
All data	Mean	1.06	1.04	1.09	1.05	1.04	1.01	1.09	1.01
	CoV	0.128	0.139	0.108	0.156	0.141	0.032	0.106	0.033
Non-slender sections	Mean	1.17	1.17	1.17	1.17	1.17	0.99	1.17	1.01
	CoV	0.123	0.123	0.123	0.123	0.123	0.023	0.121	0.029
Slender sections	Mean	0.97	0.94	1.04	0.95	0.89	1.03	1.02	1.01
	CoV	0.017	0.019	0.041	0.114	0.133	0.024	0.019	0.031

sections in different sub-groups with detailed statistical results reported in Tables 4 and 5.

4. Modifications for EWM and DSM

4.1. General

Following the evaluation of the cross-section classification and cross-section resistances, modifications on the design code concerning EWM and design approach are made. Modifications for all design codes are considered not necessary, mainly EWM specified in existing design code of Eurocode 3 was conducted. In terms of the design approaches of DSM and CSM, CSM resulted in relatively accurate predictions for cross-sectional resistances, thus modifications are mainly proposed for DSM.

4.2. Modified EWM

In this section, the modification on Eurocode 3 is presented and proposed. It should be noted sections exhibit similar structural behaviour independent of steel grades and fabrication routes for slender sections, whereas the distinguished structural performance displayed by stocky

Table 5
Comparisons of numerical results with predicted strengths based on different design methods for HexHS with nominal yield strength of 690 MPa.

No. of specimen		$N_u/N_{u,EC3}$	$N_u/N_{u,AISC}$	$N_u/N_{u,AS4100}$	$N_u/N_{u,ASCE}$	$N_u/N_{u,DSM}$	$N_u/N_{u,CSM}$	$N_u/N_{u,EC3}^*$	$N_u/N_{u,DSM}^*$
Test: 18 FE:711									
All data	Mean	0.98	0.96	1.05	1.07	0.96	1.03	1.01	1.01
	CoV	0.055	0.067	0.046	0.187	0.073	0.018	0.038	0.036
Non-slender sections	Mean	1.06	1.06	1.05	1.06	1.06	1.02	1.05	1.02
	CoV	0.045	0.046	0.041	0.045	0.046	0.017	0.039	0.021
Slender sections	Mean	0.96	0.93	1.05	1.08	0.93	1.04	1.00	1.01
	CoV	0.025	0.026	0.046	0.215	0.042	0.018	0.027	0.035

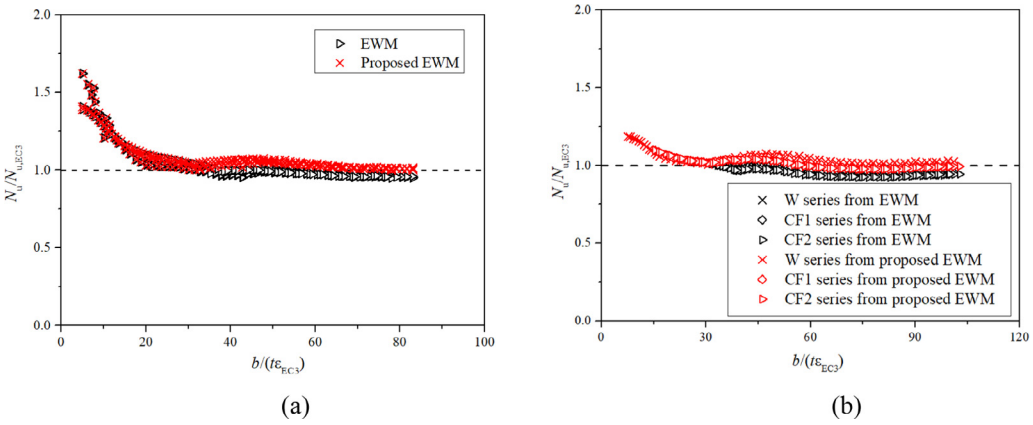

Fig. 18. Comparisons of experimental and numerical results with strength predictions from modified design code of EC3 for sections with nominal yield strength (a) 460 MPa (b) 690 MPa.

sections are mainly due to the strain hardening characteristics associated with different material properties. In the original design formulae of Eurocode 3, strain hardening is not considered for stocky sections and the attained cross-section resistance is limited to the squash load of Af_y. To have a consistent and unified prediction in line with the original design formula in Eurocode 3, no modifications are made for stocky sections. As for slender sections, the improvements are made by multiplying a factor to the cross-section slenderness in the design formula, and the boundary limits were determined by taking account of the cross-section classification slenderness proposed in Section 3.4.1, as given in Eq. (12).

$$\frac{b_{eff,EC3}}{b}=\begin{cases}1 & \text{for } \bar{\lambda}_p \le 0.5+\sqrt{0.058-0.055\psi}\\ \dfrac{0.95\bar{\lambda}_p-0.055(3+\psi)}{\bar{\lambda}_p^{\,2}} & \text{for } \bar{\lambda}_p > 0.5+\sqrt{0.058-0.055\psi}\end{cases} \tag{12}$$

The cross-sectional resistances were normalised to the predicted cross-sectional resistance based upon the modified effective width method and are plotted in Fig. 18 in comparison with the normalised counterparts based on original EWM. It is observed that improved accuracy and consistency are made from modified EWM. The mean (test and FE)-to-predicted compression resistance ratios $N_u/N_{u,pred}$, and the corresponding coefficient of variations (CoVs) are reported in Tables 4 and 5. For better comparison purposes, the cross-sectional resistances for all specimens were decomposed into slender and non-slender sections. For instance, modified EC3 results in improved accuracy and consistency with $N_u/N_{u,pred}$ equal to 1.02 whereas the original EC3 provide 0.97 on non-conservative side. Though the overall $N_u/N_{u,pred}$ derived from modified EC3* is higher than the original one, the predicted strengths are more reliable. For sections with nominal yield strength of 690 MPa, the mean values of $N_u/N_{u,pred}$ have been improved from 0.98 to 1.01, with corresponding CoVs from 0.055 to 0.038 whereas $N_u/N_{u,pred}$ for slender sections have been improved from 0.96 to 1.00 with corresponding CoVs from 0.025 to 0.027.

4.3. Modified DSM

The original DSM is employed in the North American design code of AISI S100-16, without the inclusion of the strain hardening effect, particularly for sections subject to large plastic deformation. For stocky sections of the stub column specimens, strains have developed into hardening stage after yield plateau. From the above evaluation analysis, it is known that the current DSM generally provide non-conservatism predictions for slender sections and over-conservatism for stocky sections for both two steel grades. Hence, modifications are made to improve the accuracy and consistency. To address the large degree of conservatism for stocky sections which enters plastic stage with large deformation, new design formulae are proposed to replace the original horizontal yield line with a bi-linear expression comprising sections slenderness and correlated factors accounting for material characteristics, as given in Eq. (13).

$$\frac{N_{DSM}}{N_y}=\begin{cases}1+(1-d_1\lambda_p)d_2 & \text{for } 0.05<\lambda_p\le 0.40\\ 1+(1-d_3\lambda_p)d_4 & \text{for } 0.40<\lambda_p\le 0.65\\ (1-\dfrac{0.22}{\lambda_p^{0..901}})\dfrac{1}{\lambda_p^{0..901}} & \text{for } \lambda_p>0.65\end{cases} \tag{13}$$

where the material coefficients of d_1, d_2, d_3, and d_4 are used to account for the effect of the strain hardening of the used material at different slenderness ranges. Based on regression analysis, the coefficients of $d_1 = 2.31$ and $d_2 = 0.83$ are proposed for sections with slenderness ranging between 0.05 and 0.40, while $d_3 = 1.6$ and $d_4 = 0.18$ are proposed for sections with slenderness ranging between 0.40 and 0.65.

The accuracy and suitability of the proposed modifications to DSM were assessed by comparing the experimental and numerical results with the predicted cross-sectional resistances calculated based on the modified DSM. As can be seen in Fig. 19, the normalised cross-sectional resistance ratio between ultimate load N_u and predicted cross-sectional resistance from modified DSM $N_{u,pred}$ shows notable improvement. The mean values of $N_u/N_{u,DSM}^*$ for sections with steel grades of 460 MPa and 690 MPa are 1.01 and 1.02 respectively with the corresponding

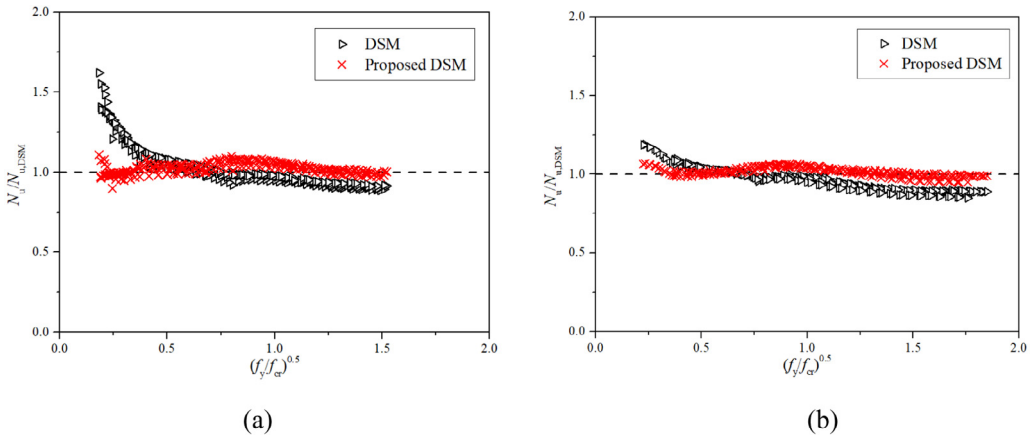

Fig. 19. Comparisons of experimental and numerical results with strength predictions from modified design approach of DSM for sections with nominal yield strength (a) 460 MPa (b) 690 MPa.

Table 6
Reliability analysis results for HSS HexHS stub columns under pure compression for sections with nominal yield strength of 460 MPa.

Steel grade	No. of specimens		Design codes and design methods							
			EC3	AISC 360	AS 4100	DSM	CSM	ASCE	EC3*	DSM*
Q460	All data: 729	$k_{d,n}$	3.107	3.107	3.107	3.107	3.107	3.107	3.107	3.107
		b	0.991	0.965	1.048	0.962	1.022	0.963	1.042	1.016
		V_δ	0.117	0.127	0.099	0.131	0.047	0.153	0.098	0.032
		V_r	0.127	0.137	0.112	0.141	0.070	0.161	0.110	0.060
		γ_{Mo}	1.320	1.390	1.184	1.421	1.060	1.519	1.187	1.018
	Sub-set: 140 (non-slender)	$k_{d,n}$	3.111	3.111	3.111	3.111	3.111	3.111	3.111	3.111
		b	1.091	1.091	1.091	1.091	0.993	1.091	1.091	1.018
		V_δ	0.118	0.119	0.119	0.119	0.051	0.119	0.117	0.035
		V_r	0.129	0.129	0.129	0.129	0.072	0.129	0.127	0.062
		γ_{Mo}	1.205	1.207	1.207	1.207	1.102	1.207	1.199	1.034
	Sub-set: 589 (slender)	$k_{d,n}$	3.163	3.163	3.163	3.163	3.163	3.163	3.163	3.163
		b	0.971	0.943	1.042	0.941	1.032	0.938	1.032	1.026
		V_δ	0.017	0.019	0.042	0.033	0.025	0.114	0.020	0.031
		V_r	0.054	0.055	0.066	0.061	0.057	0.125	0.055	0.060
		γ_{Mo}	1.059	1.096	1.028	1.118	1.007	1.381	1.001	1.015

Table 7
Reliability analysis results for HSS HexHS stub columns under pure compression for sections with nominal yield strength of 690 MPa.

Steel grade	No. of specimens		Design codes and design methods							
			EC3	AISC 360	AS 4100	DSM	CSM	ASCE	EC3*	DSM*
Q690	All data: 711	$k_{d,n}$	3.108	3.108	3.108	3.108	3.108	3.108	3.108	3.108
		b	0.961	0.938	1.041	0.932	1.029	1.012	1.011	1.018
		V_δ	0.054	0.065	0.046	0.071	0.018	0.175	0.037	0.041
		V_r	0.074	0.083	0.069	0.088	0.054	0.182	0.064	0.066
		γ_{Mo}	1.195	1.202	1.037	1.233	0.998	1.546	1.049	1.023
	Sub-set: 122 (non-slender)	$k_{d,n}$	3.163	3.163	3.163	3.163	3.163	3.163	3.163	3.163
		b	1.031	1.036	1.035	1.036	1.023	1.035	1.041	1.018
		V_δ	0.044	0.046	0.045	0.045	0.017	0.044	0.042	0.022
		V_r	0.068	0.069	0.068	0.068	0.054	0.068	0.067	0.056
		γ_{Mo}	1.091	1.041	1.039	1.039	1.004	1.039	1.029	1.005
	Sub-set: 589 (slender)	$k_{d,n}$	3.111	3.111	3.111	3.111	3.111	3.111	3.111	3.111
		b	0.951	0.932	1.047	0.919	1.028	1.013	1.014	1.018
		V_δ	0.024	0.026	0.045	0.055	0.017	0.202	0.033	0.046
		V_r	0.057	0.057	0.068	0.075	0.054	0.208	0.061	0.068
		γ_{Mo}	1.092	1.117	1.025	1.197	0.998	1.687	1.041	1.026

values of CoV 0.033, and 0.042 respectively. Improved accuracy and consistency for cross-sectional predictions are evidenced by the mean values of the experimental and numerical strength over the corresponding predictions being closer to the unity and the possession of lower values of CoV, as shown in Tables 4 and 5.

5. Reliability analysis

In this section, the reliability level and required partial factor for the existing design codes, design approaches, and proposed modified expressions for high strength steel hexagonal hollow section stub columns

using the first order reliability method (FORM) set out in EN 1990 [69]. The variability parameters (i.e., the ratio between the mean and nominal values X_m/X_n, where X represents the basic variables, and the corresponding CoV) of the basic material and geometric properties, where taken in accordance with Annex E of prEN 1993-1-1 [70]. The material over-strength ratio $f_{y,mean}/f_{y,nom} = 1.15$ was used for HSS Q460 and $f_{y,mean}/f_{y,nom} = 1.10$ was used for sections with 690 MPa as per Annex E of prEN 1993-1-1 [70]. The CoV of the geometric properties were taken as 0.009 and 0.025 for width and thickness respectively. The key statistical parameters for the design codes and design approaches are summarised in Tables 6 and 7, including the number of tests and numerical models, the design fractile factor $k_{d,n}$, the mean value of the correction factor b, the coefficient of variation of the tests and FE models relative to the resistance model V_δ, the combined coefficient of variation incorporating both model and basic variable uncertainties V_r and the required partial safety factor γ_{M0}. The correction factor b can be derived based on least squares analysis between the resistance capacities from tests and design predictions from resistance model, as shown in Eq. (14), where r_e is the experimental results and r_t is the theoretical results of the resistance model.

$$b = \frac{\sum r_e r_t}{\sum {r_t}^2} \tag{14}$$

It shows that the AS 4100 require lower partial factor than EC 3 and AISC 360-16 for HSS HexHS with three fabrication routes for both sections with nominal yield strength of 460 MPa and 690 MPa. In terms of the design approaches, the required partial factors for CSM are lower than the design approach of DSM, which is close to the unity for section with yield strength of 460 MPa, as shown in Table 6. The modified EC3 method generates improved reliability compared with the original one with reduced required partial factor. It can be observed that the overall partial factors required for modified EC3* are 1.187 and 1.049 for sections with yield strength of 690 MPa and 460 MPa respectively. To further illustrate the level of improvement in cross-sectional resistance design, the obtained results were divided into two sub-sets of slender and non-slender groups. For the group of slender sections, partial factor of 1.001 and 1.041 are determined with relatively lower V_δ, between obtained results and resistance models in comparison to the original EC3 design formulae. In terms of the design approach DSM, modified design formulae provide lower required partial factors than the original method with 1.018 and 1.045 respectively for sections of 460 MPa and 690 MPa respectively, primarily attributed to the lower values of the V_δ determined from modified methods, leading to notable improvement in cross-section predictions and increased consistency.

6. Conclusion

A comprehensive numerical investigation into the local buckling behaviour and design of the HSS HexHS stub columns under pure compression has been conducted and presented in this paper. The finite element models were developed firstly and validated against the experimental results for HSS HexHS with three different fabrication routes. Extensive parametric studies were subsequently conducted to expand the numerical results covering a larger spectrum of geometries and cross-sectional slenderness and different steel grades. The obtained numerical results together with the experimental results were utilised to assess the accuracy and applicability of the current design codes of Eurocode 3, ANSI/AISC 360-16 and AS 4100, ASCE/SEI 48 as well as the design approaches including DSM, CSM. Based upon the evaluations presented in this paper, the following conclusions can be made:

(a) The current codified slenderness limits in structural steel design standards of EC3, AISC 360-16 and AS 4100 cannot be simply extended to cover the cross-section classification of HSS HextHS stub columns under compression. A new cross-section slenderness yield limit value of $\bar{\lambda}_p = 0.55$ is proposed for HSS HexHS under pure compression.

(b) In terms of cross-sectional resistances, all design codes exhibit over-conservatism for stocky sections as strain hardening effect is not included in design codes. For slender sections, non-conservatism was observed from the existing design standards of EC3 and AISC 360-16, whereas conservative predictions were provided by AS 4100.

(c) Though ASCE/SEI 48 provide design provisions for HexHS, the most scattered and conservative predictions are provided by ASCE/SEI 48 for slender sections.

(d) Compared with design codes, design approach of CSM provides more accurate and consistent predictions for both stocky and slender sections, primarily attributed to the more accurate boundary limits and the strain hardening effect is accounted for in deformation-based design formulae.

(e) The modified design code of EC3 and design approach of DSM provide more accurate and reliable design than the original design approaches. The modified DSM can take strain hardening into account, and the characteristics of the HSS material applicable to DSM is proposed.

CRediT authorship contribution statement

Jun-zhi Liu: Writing – original draft, Validation, Investigation, Conceptualization. **Han Fang:** Writing – review & editing. **Jiachen Guo:** Writing – review & editing. **Shuai Li:** Writing – review & editing. **Tak-Ming Chan:** Writing – review & editing, Supervision, Funding acquisition, Conceptualization.

Declaration of competing interest

The authors declare that they have no known competing financial interests or personal relationships that could have appeared to influence the work reported in this paper.

Data availability

Data will be made available on request.

Acknowledgement

The research work presented in this paper was supported by a grant from the Research Grants Council of the Hong Kong Special Administrative Region, China (Project no. 15218918).

References

[1] N. Baddoo, Briefing: More from less–greater materials efficiency using high-strength steels, Proc. Inst. Civ. Eng.-Struct. Build. 175 (5) (2022) 359–362.
[2] Z.-Y. Zhou, Y.-Y. Chen, M.C.H. Yam, K. Ke, X.-Z. He, Experimental investigation of a high strength steel frame with curved knee braces subjected to extreme earthquakes, Thin-Walled Struct. 185 (2023) 110596.
[3] N. Baddoo, A. Chen, High Strength Steel Design and Execution Guide, Vol. 398, SCI (the Steel Construction 397 Institute), 2020.
[4] M.-X. Xiong, J.R. Liew, Experimental study to differentiate mechanical behaviours of TMCP and QT high strength steel at elevated temperatures, Constr. Build. Mater. 242 (2020) 118105.
[5] Y. Shin, S. Kang, H. Lee, Fracture characteristics of TMCP and QT steel weldments with respect to crack length, Mater. Sci. Eng. A 434 (1–2) (2006) 365–371.
[6] G.-Q. Li, L.-X. Song, Mechanical properties of TMCP Q690 high strength structural steel at elevated temperatures, Fire Saf. J. 116 (2020) 103190.
[7] H. Ban, G. Shi, Y. Shi, Y. Wang, Overall buckling behavior of 460 MPa high strength steel columns: Experimental investigation and design method, J. Constr. Steel Res. 74 (2012) 140–150.
[8] H. Ban, G. Shi, Overall buckling behaviour and design of high-strength steel welded section columns, J. Constr. Steel Res. 143 (2018) 180–195.
[9] G. Shi, W. Zhou, Y. Bai, C. Lin, Local buckling of 460 MPa high strength steel welded section stub columns under axial compression, J. Constr. Steel Res. 100 (2014) 60–70.
[10] G. Shi, W. Zhou, C. Lin, Experimental investigation on the local buckling behavior of 960 MPa high strength steel welded section stub columns, Adv. Struct. Eng. 18 (3) (2015) 423–437.
[11] N. Schillo, M. Feldmann, Interaction of local and global buckling of box sections made of high strength steel, Thin-Walled Struct. 128 (2018) 126–140.

[12] Y.-B. Wang, G.-Q. Li, S.-W. Chen, F.-F. Sun, Experimental and numerical study on the behavior of axially compressed high strength steel box-columns, Eng. Struct. 58 (2014) 79–91.
[13] S.-D. Nie, S.-B. Kang, L. Shen, B. Yang, Experimental and numerical study on global buckling of Q460GJ steel box columns under eccentric compression, Eng. Struct. 142 (2017) 211–222.
[14] S.-B. Kang, B. Yang, X. Zhou, S.-D. Nie, Global buckling behaviour of welded Q460GJ steel box columns under axial compression, J. Constr. Steel Res. 140 (2018) 153–162.
[15] T.-J. Li, G.-Q. Li, S.-L. Chan, Y.-B. Wang, Behavior of Q690 high-strength steel columns: Part 1: Experimental investigation, J. Constr. Steel Res. 123 (2016) 18–30.
[16] Z. Huang, D. Li, B. Uy, H.-T. Thai, C. Hou, Local and post-local buckling of fabricated high-strength steel and composite columns, J. Constr. Steel Res. 154 (2019) 235–249.
[17] D. Li, Z. Huang, B. Uy, H.-T. Thai, C. Hou, Slenderness limits for fabricated S960 ultra-high-strength steel and composite columns, J. Constr. Steel Res. 159 (2019) 109–121.
[18] M.-T. Chen, B. Young, Beam–column tests of cold-formed steel elliptical hollow sections, Eng. Struct. 210 (2020) 109911.
[19] X. Meng, L. Gardner, Testing of hot-finished high strength steel SHS and RHS under combined compression and bending, Thin-Walled Struct. 148 (2020) 106262.
[20] J. Wang, S. Afshan, N. Schillo, M. Theofanous, M. Feldmann, L. Gardner, Material properties and compressive local buckling response of high strength steel square and rectangular hollow sections, Eng. Struct. 130 (2017) 297–315.
[21] X.L. Zhao, Section capacity of very high strength (VHS) circular tubes under compression, Thin-Walled Struct. 37 (3) (2000) 223–240.
[22] H. Jiao, X.L. Zhao, Imperfection, residual stress and yield slenderness limit of very high strength (VHS) circular steel tubes, J. Constr. Steel Res. 59 (2) (2003) 233–249.
[23] J.-L. Ma, T.-M. Chan, B. Young, Experimental investigation on stub-column behavior of cold-formed high-strength steel tubular sections, J. Struct. Eng. 142 (5) (2016) 04015174.
[24] J.-L. Ma, T.-M. Chan, B. Young, Cold-formed high-strength steel rectangular and square hollow sections under combined compression and bending, J. Struct. Eng. 145 (12) (2019) 04019154.
[25] J.L. Ma, T.M. Chan, B. Young, Design of cold-formed high-strength steel tubular stub columns, J. Struct. Eng. 144 (6) (2018) 04018063.1-04018063.10.
[26] X. Meng, L. Gardner, Cross-sectional behaviour of cold-formed high strength steel circular hollow sections, Thin-Walled Struct. 156 (2020) 106822.
[27] T.M. Chan, L. Gardner, Compressive resistance of hot-rolled elliptical hollow sections, Eng. Struct. 30 (2) (2008) 522–532.
[28] M.-T. Chen, B. Young, Material properties and structural behavior of cold-formed steel elliptical hollow section stub columns, Thin-Walled Struct. 134 (2019) 111–126.
[29] M.-T. Chen, B. Young, Structural performance of cold-formed steel elliptical hollow section pin-ended columns, Thin-Walled Struct. 136 (2019) 267–279.
[30] M.-T. Chen, B. Young, Numerical analysis and design of cold-formed steel elliptical hollow sections under combined compression and bending, Eng. Struct. 241 (2021) 112417.
[31] M.-T. Chen, B. Young, Cross-sectional behavior of cold-formed steel semi-oval hollow sections, Eng. Struct. 177 (2018) 318–330.
[32] M.-T. Chen, B. Young, Beam–column design of cold-formed steel semi-oval hollow non-slender sections, Thin-Walled Struct. 162 (2021) 107376.
[33] J.-H. Zhu, B. Young, Cold-formed-steel oval hollow sections under axial compression, J. Struct. Eng. 137 (7) (2011) 719–727.
[34] J.-Z. Liu, H. Fang, S. Chen, T.-M. Chan, Material properties and residual stresses of high strength steel hexagonal hollow sections, J. Constr. Steel Res. 190 (2022) 107061.
[35] J.-Z. Liu, H. Fang, T.-M. Chan, Structural behaviour of high strength steel hexagonal hollow section stub columns under axial compression, Eng. Struct. 268 (2022) 114653.
[36] J.-Z. Liu, H. Fang, T.-M. Chan, Investigations on material properties and residual stresses in cold-formed high strength steel irregular hexagonal hollow sections, Thin-Walled Struct. 176 (2022) 109220.
[37] J.-Z. Liu, H. Fang, T.-M. Chan, Experimental investigations on material properties and stub column behaviour of high strength steel irregular hexagonal hollow sections, J. Constr. Steel Res. 196 (2022) 107343.
[38] J.-Z. Liu, H. Fang, T.-M. Chan, Numerical investigation on local buckling behaviour of cold-formed high strength steel irregular hexagonal hollow section stub columns, Thin-Walled Struct. 185 (2023) 110571.
[39] J. Chen, J.-Y. Zhu, T.-M. Chan, Experimental and numerical investigation on stub column behaviour of cold-formed octagonal hollow sections, Eng. Struct. 214 (2020) 110669.
[40] H. Fang, T.-M. Chan, B. Young, Behavior of octagonal high-strength steel tubular stub columns, J. Struct. Eng. 145 (12) (2019) 04019150.
[41] J.Z. Liu, H. Fang, T.-M. Chan, Experimental and numerical investigations on stub column behaviour of cold-formed high strength steel irregular octagonal hollow sections, Thin-Walled Struct. 180 (2022) 109770.
[42] W. Xu, L.-H. Han, W. Li, Performance of hexagonal CFST members under axial compression and bending, J. Constr. Steel Res. 123 (2016) 162–175.
[43] ANSI/AISC 360-16, Specification for Structural Steel Buildings, American Institute of Steel Construction (AISC), Chicago, 2016.
[44] AS 4100-1998(R2016), Steel Structures (Reconfirmed 2016 Incorporating Amendment No. 1), AS 4100, Australian Standard, Sydney, Australia, 2016.
[45] EN 1993-1-1, Eurocode 3: Design of Steel Structures – Part 1.1: General Rules and Rules for Buildings, European Committee for Standardization (CEN), Brussels, 2005.
[46] ASCE/SEI 48-11, Design of Steel Transmission Pole Structures, American Society of Civil Engineers, Reston, Virginia, 2011.
[47] EN 1993-1-12, Eurocode 3: Design of Steel Structures – Part 1–12: Additional Rules for the Extension of EN 1993 Up to Steel Grades S700, European Committee for Standardization (CEN), Brussels, 2007.
[48] EN 1993-1-5, Eurocode 3: Design of Steel Structures – Part 1–5: Plated Structural Elements, European Committee for Standardization (CEN), Brussels, 2006.
[49] ABAQUS/Standard. Version 6.14-1, K. a. S. Hibbit, U.S.A..
[50] T.-M. Chan, X.-L. Zhao, B. Young, Cross-section classification for cold-formed and built-up high strength carbon and stainless steel tubes under compression, J. Constr. Steel Res. 106 (2015) 289–295.
[51] R. Gonçalves, D. Camotim, Elastic buckling of uniformly compressed thin-walled regular polygonal tubes, Thin-Walled Struct. 71 (2013) 35–45.
[52] R. Gonçalves, A.D. Martins, D. Camotim, Elastic bifurcation, postbuckling behavior, and collapse of thin-walled regular polygonal columns, J. Eng. Mech. 149 (2023) 04022090.
[53] M. Theofanous, T.M. Chan, L. Gardner, Structural response of stainless steel oval hollow section compression members, Eng. Struct. 31 (4) (2009) 922–934.
[54] J.-Z. Liu, S. Chen, T.-M. Chan, Testing, numerical modelling and design of Q690 high strength steel welded T-section stub columns, Eng. Struct. 259 (2022) 114142.
[55] J.-Z. Liu, S. Chen, T.-M. Chan, Experimental and numerical investigations of hybrid high strength steel welded T-section stub columns with Q690 flange and Q460 web, Thin-Walled Struct. 177 (2022) 109403.
[56] J. Chen, H. Liu, T.-M. Chan, Material properties and residual stresses of cold-formed octagonal hollow sections, J. Constr. Steel Res. 170 (2020) 106078.
[57] J.-Z. Liu, S. Chen, T.-M. Chan, Hybrid welded T-section stub columns with Q690 flange and Q355 web: Testing, Model. Des. Eng. Struct. 274 (2023) 115142.
[58] S. Chen, J. z. Liu, T.-M. Chan, Material properties and residual stresses of welded high strength steel and hybrid I-sections, Eng. Struct. 276 (2023) 115293.
[59] L. Schaper, T. Tankova, L.S. da Silva, M. Knobloch, A novel residual stress model for welded I-sections, J. Constr. Steel Res. 188 (2022) 107017.
[60] B.W. Schafer, T. Peköz, Computational modeling of cold-formed steel: characterizing geometric imperfections and residual stresses, J. Constr. Steel Res. 47 (3) (1998) 193–210.
[61] B.W. Schafer, Advances in the direct strength method of cold-formed steel design, Thin-Walled Struct. 140 (2019) 533–541.
[62] L. Gardner, The continuous strength method, Proc. Inst. Civ. Eng. Struct. Build. 161 (3) (2008) 127–133.
[63] O. Zhao, L. Gardner, B. Young, Behaviour and design of stainless steel SHS and RHS beam–columns, Thin-Walled Struct. 106 (2016) 330–345.
[64] X. Yun, L. Gardner, Numerical modelling and design of hot-rolled and cold-formed steel continuous beams with tubular cross-sections, Thin-Walled Struct. 132 (2018) 574–584.
[65] X. Yun, L. Gardner, N. Boissonnade, The continuous strength method for the design of hot-rolled steel cross-sections, Eng. Struct. 157 (2018) 179–191.
[66] X. Lan, J. Chen, T.-M. Chan, B. Young, The continuous strength method for the design of high strength steel tubular sections in compression, Eng. Struct. 162 (2018) 177–187.
[67] X. Yun, L. Gardner, Stress–strain curves for hot-rolled steels, J. Constr. Steel Res. 133 (2017) 36–46.
[68] S. Chen, H. Fang, J.-Z. Liu, T.-M. Chan, Design for local buckling behaviour of welded high strength steel I-sections under bending, Thin-Walled Struct. 172 (2022) 108792.
[69] EN 1990, Eurocode - Basis of Structural Design, European Committee for Standardization (CEN), Brussels, Belgium, 2002.
[70] prEN1993-1-1, Eurocode 3: Design of Steel Structures – Part 1-1: General Rules and Rules for Buildings, Final Document, European Committee for Standardization (CEN), Brussels, 2020.